Single-crystal to Single-crystal transformations of MOF-supported, site-isolated trigonal planar Cu(I) complexes with labile ligands

Ricardo A. Peralta,[a] Michael T. Huxley,[a] Jorge Albalad,[a] Christopher J. Sumby[a] and Christian J. Doonan[a]**

a. Centre for Advanced Nanomaterials and Department of Chemistry, The University of Adelaide, North Terrace, Adelaide, SA 5000, Australia. Email: christopher.sumby@adelaide.edu.au (CJS); christian.doonan@adelaide.edu.au (CJD)

Abstract

Transition metal complexes bearing labile ligands can be difficult to isolate and study in solution due to unwanted dinucleation or ligand substitution reactions. Metal-organic Frameworks (MOFs) provide a unique matrix that allows site isolation and stabilization of well-defined transition metal complexes that may be of importance as moieties for gas adsorption or catalysis. Herein we report the development of an *in-situ* anion metathesis strategy which facilitates the post-synthetic modification of Cu(I) complexes appended to a porous, crystalline MOF. By exchanging coordinated chloride for weakly coordinating anions in the presence of carbon monoxide or ethylene, a series of labile MOF-appended Cu(I) complexes featuring carbon monoxide or ethylene ligands are prepared and structurally characterized using X-ray crystallography. These complexes have an uncommon trigonal planar geometry due to the absence of coordinating solvents. The porous host framework allows small and moderately sized molecules to access the isolated Cu(I) sites and displace the "place-holder" CO ligand, mirroring the ligand exchange processes involved in Cu-centred catalysis.

Introduction

Metal-organic frameworks (MOFs) are a class of porous, crystalline materials that are assembled via a building block approach from metal-based nodes and organic links.[1-3] This synthetic strategy allows for metal-binding ligand moieties such as, 2,2'-bipyidine,[4-8] porphyrins,[9] bis and tris pyrazoles[10-14] and phosphorous-based

systems,[15-17] to be readily incorporated into the MOF architecture as structural units.[18, 19] As a result, the MOF pore network can be furnished with transition metal complexes to enhance specific performance characteristics, e.g., gas adsorption[4] and catalysis.[7, 12, 14, 17, 20] The chemistry of metal complexes anchored to a MOF lattice is distinct from the solution phase as it provides a pathway to site-isolation that obviates, typically, undesired dinucleation reactions and can facilitate site-selective chemistry.[4, 11, 15, 18, 19, 21, 22] Furthermore, in the crystalline solid-state well-defined complexes replete with weakly coordinating ligands, that would be displaced by solvent molecules in solution, can be accessed and precisely characterized via diffraction methods.[23-26] Thus, such metalated MOFs represent excellent structural models for studying the fundamental inorganic reaction processes that underpin catalytic reactions.[27]

Previous work has shown that the stabilization of labile ligands and their chemistry can be structurally elucidated by examining single-crystal to single-crystal (SC-SC) reactions in solid-state molecular systems.[28-30] For example, Brookhart and co-workers reported that the labile dinitrogen ligand of an Ir(I) pincer complex, [Ir(L^{PCP})(N_2)] (Figure 1a, where L^{PCP} = C_6H_4-1,3-[OP(C_6H_2-2,4,6-$(CF_3)_3$)$_2$]$_2$, underwent exchange via a dissociative mechanism.[31] In addition, Weller and co-workers showed that a Rhodium σ–alkane complex could be synthesized by carrying out a solid-gas reaction on crystals of [Rh(dcype)(norbornane)][BAr^F_4] (Figure 1b, where dcype = 1,2-bis(dicyclohexylphosphino)ethane).[23] Both examples highlight that to explore the reactivity of metal centers isolated within a crystalline matrix, pore networks that allow for the diffusion of molecular substrates are required.[24, 28] In molecular crystals, pore structures are generated by crystal packing forces and thus cannot be tailored via *a priori* design principles. Additionally, they are unstable towards a broad spectrum of reaction conditions.[28] In contrast to molecular crystals, MOFs offer robust architectures and the potential to control pore dimensions and functionality through careful selection of the organic building units. Indeed, we have demonstrated that a Mn(II)-based MOF, **MnMOF-1**; ([Mn_3L_2L'] (where L = L' = bis(4-carboxyphenyl-(3,5-dimethylpyrazol-1-yl))methane) is an excellent platform material to study inorganic

chemistry in the crystalline solid-state. Due to the flexibility of the N,N'-chelating ligand, **MnMOF-1** readily accommodates the subtle structural transformations that accompany post-synthetic metalation and subsequent metal-centered reactions[10, 12-14, 32] without losing long-range order.

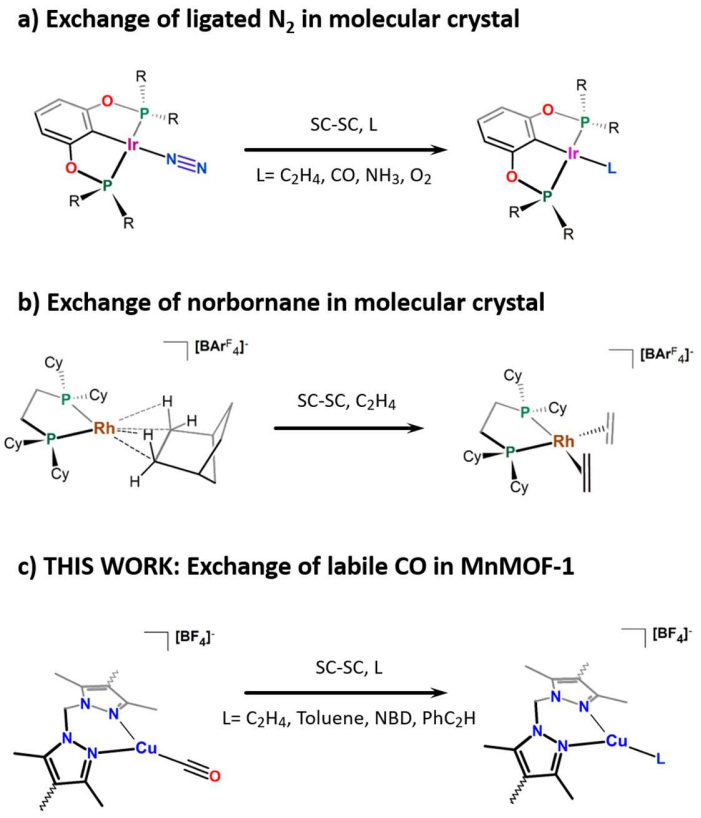

Figure 1. Examples of previous SC-SC studies of ligand exchange at labile transition metal complexes in the solid state; exchange of small gaseous molecules at an Ir(I) dinitrogen complex **(a)** and a Rh(I) σ-alkane complex **(b)** reported by Brookhart *et al.*[31] and Weller *et al.*[23] respectively. This work **(c)** involves ligand exchange occurring at a labile Cu(I) carbonyl complex housed within **MnMOF-1**.

Copper(I) exhibits diverse coordination chemistry and readily participates in both one- and two-electron transfer reactions.[33] As a result, Cu(I) complexes have been widely explored for their applications in catalytic oxidative coupling reactions. Furthermore, Cu(I) complexes are of great interest in homogeneous catalysis

due to their versatility, relative earth abundance, compared to precious metal systems, and low toxicity. In MOF chemistry, Cu(I) cations have been employed to enhance gas separation performance[34] and as single atom catalytic sites,[11, 35] in both cases free coordination sites are crucial to functionality. Thus, developing synthetic methods that lead to the isolation of coordinatively unsaturated copper (I) sites within MOFs is an important step towards expanding this chemistry. Herein, we employ an *in-situ* anion metathesis strategy to realize a series of trigonal planar Cu(I) complexes (Figure 2) bearing weakly coordinated ligands. The crystallographic characterization of such Cu(I) complexes is typically elusive; however, the MOF matrix offers a unique environment for their isolation and stabilization. By virtue of the highly crystalline and robust host framework we were able to map the ligand exchange processes at the site-isolated Cu(I) moieties within **MnMOF-1** via single crystal X-ray crystallography (SCXRD) and thus advance the fundamental chemistry required to explore novel Cu centered chemistry in MOFs.

Results and Discussion

Synthesis of labile Cu(I) complexes in MnMOF-1

A promising facet of MOF chemistry is their potential as platforms for studying the exchange of small, labile molecules bound to well-defined, site isolated complexes; a role foreshadowed by their intrinsically high crystallinity, tunable structure metrics and permanent porosity.[36-40] Indeed, such insights can inform the development of MOFs for applications in selective gas adsorption and heterogeneous catalysts. We envisaged that an '*in situ* anion metathesis' strategy could generate open coordination sites within **MnMOF-1** by directly exchanging coordinated halide anions for weakly coordinating anions. By carrying out anion exchange in the presence of small gas molecules a variety metal complexes with highly labile ligands can be realized. This approach is effectively a MOF-centric adaptation of anion metathesis, a pervasive process in organometallic chemistry.[41] The preponderance of Cu(I) to adopt a wide range of coordination geometries[42, 43] (tetrahedral,[44-

[47] trigonal planar,[44, 45] digonal[48, 49]) and known capacity to form labile complexes with carbon monoxide and ethylene;[50, 51] motivated us to explore our strategy using Cu(I) functionalized **MnMOF-1**. Many Cu(I) catalysts, such as those studied for carbene and nitrene insertion, are based on complexes featuring labile ligands which allow facile binding and activation of the reagent molecules such as organic azides and diazoacetates.[11, 52-57] As such, stabilizing weakly-ligated complexes via site-isolation within a robust crystalline host is of significant interest.[11]

Our entry point to Cu(I) chemistry in **MnMOF-1** was via direct metalation with CuCl. Exposure of **MnMOF-1** to CuCl in acetonitrile at 4°C resulted in a color change in the crystals from colorless to pale yellow. SCXRD revealed the formation of a tetrahedral N,N'-chelated Cu(I) complex, which exists as a mixture of the charged bis-acetonitrile and neutral mono-acetonitrile complexes **MnMOF-1**·[$Cu(MeCN)_2$]Cl and **MnMOF-1**·[CuCl(MeCN)], respectively. The material, designated **MnMOF-1**·[CuCl(MeCN)] for simplicity, crystallizes in the space group $P2_1/m$ (Figure 2). The crystallographically distinct Cu(I) centers are highly disordered (See S3.2 for refinement details), precluding analysis of the respective bond lengths; however analogous structural motifs have been reported.[47, 58] Energy Dispersive X-ray (EDX) analysis confirmed quantitative metalation (Mn:Cu:Cl = 3:1:1, see Table S1).

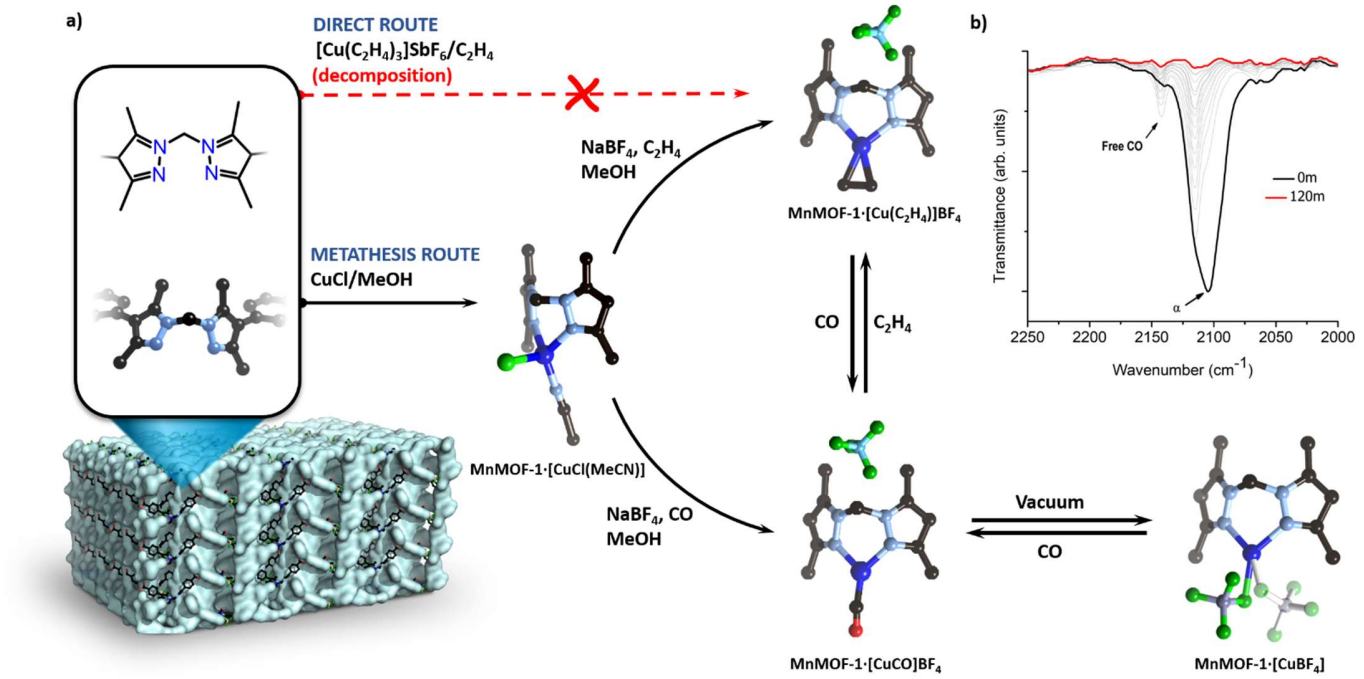

Figure 2. (a) Accessing **MnMOF-1**·[$Cu(C_2H_4)$]BF_4 via the direct route leads to decomposition of [$Cu(C_2H_4)_3$]SbF_6. Only *via* the metathesis route, which involves metalation of **MnMOF-1** with CuCl and subsequent anion metathesis with $NaBF_4$ in the presence of ethylene or CO, can the corresponding labile complexes be obtained. **MnMOF-1**·[CuCO]BF_4 loses CO under vacuum to yield the BF_4 complex **MnMOF-1**·[$CuBF_4$], with the coordinated BF_4 is disordered over four crystallographically distinct positions (two generated by a mirror plane that bisects the Cu center). IR spectra collected under vacuum clearly indicates the quantitative loss of coordinated CO and transient formation of free CO in the MOF pores **(b)**. Hydrogen atoms have been omitted for clarity; the MOF backbone is represented by a blue Van der Waals surface. (C, black; N, lavender; O, red; Cu, blue; B, pale blue; F, green; S, yellow; Cl, lime-green; P, pink).

To examine the potential of the *in-situ* anion metathesis methodology in MOFs, tetrafluoroborate was introduced as the weakly-coordinating anion and ethylene as the labile placeholder ligand. **MnMOF-1**·[CuCl(MeCN)] crystals were soaked in a saturated methanol solution of $NaBF_4$ under 4 bar of ethylene for

3 days. The resulting colorless MOF crystals were then subjected to EDX analysis to ascertain the extent of Cl substitution by BF_4. The data showed a Mn:Cu:Cl ratio of 3:1:0, confirming quantitative anion exchange and retention of the Cu center within the host framework (see Table S1). It is worth noting, attempts to exchange the Cl for BF_4 in dry methanol under an inert gas were unsuccessful (EDX analysis revealed a 3:1:1 Mn:Cu:Cl ratio). The bulk crystallinity and phase purity of the material was confirmed by PXRD data (Figure S3). To elucidate the Cu(I) coordination environment, SCXRD data was collected using Synchrotron radiation.[59, 60] Close inspection of the diffraction data revealed a trigonal planar Cu(I) complex comprised of two N atoms from L and an ethylene ligand; **MnMOF-1**·$[Cu(C_2H_4)]BF_4$. The Cu–C bond lengths of 2.125(16) and 2.036(15) Å are comparable with analogous molecular complexes.[50, 61, 62] Analogous to our previous studies,[10, 12, 63] the charge balancing anion (BF_4^-) occupies a pocket within the MOF pore adjacent to the N,N'-chelated Cu(I) center. Numerous three coordinate, N,N'-chelated Cu(I) ethylene complexes have been reported in literature and structurally characterized,[45, 50, 62, 64] highlighting the relative stability of the copper-ethylene bond when suitably protected.

Simultaneously, we explored the direct metalation of **MnMOF-1** with the precursor $[Cu(C_2H_4)_3]SbF_6$ to generate **MnMOF-1**·$[Cu(C_2H_4)]SbF_6$. Despite this being a viable approach for synthesis of molecular complexes,[65] efforts to metalate **MnMOF-1** with $[Cu(C_2H_4)_3]SbF_6$ proved unsuccessful due to decomposition of the tris-ethylene precursor in solution. Next, we expanded our methodology to a more labile ligand, carbon monoxide (CO). [66-68] Cu(I) exhibits a weak interaction with CO due to negligible backbonding, making it an ideal 'placeholder' ligand. This property is emphasized by the observation of ν(C≡O) stretches which are higher than that of free CO (2143 cm^{-1}) in several reported Cu(I) carbonyl complexes.[67, 69, 70] **MnMOF-1**·[CuCl] crystals were exposed to CO (4 bar) during ion-exchange with $NaBF_4$, during which a new stretch appeared at 2105 cm^{-1} in the IR spectrum, indicating formation of a new Cu(I) carbonyl species. As anticipated, the ν(C≡O) stretch is close to that of free CO due to minimal backbonding from Cu(I) to the CO

π* orbital.[44, 51, 71] To establish the extent of anion exchange, EDX analysis was performed which revealed the absence of chloride within the sample (see Table S1). Additionally, PXRD confirmed that bulk crystallinity is retained after the ligand exchange process. (Figure S3). We note that exposure of **MnMOF-1**·[CuCl] to a CO atmosphere only (i.e., no anion present) failed to elicit formation of a carbonyl complex; the IR spectra showed an absence of ν(C≡O) stretches. This suggests that the replacement of Cl by CO occurs via a dissociative pathway and provides confirmation of the weak Cu(I)–CO interaction. Following anion exchange chemistry under CO, the crystals remained in satisfactory condition for SCXRD studies. Careful analysis of the data revealed the formation of a trigonal planar Cu(I) carbonyl complex, **MnMOF-1**·[CuCO]BF_4 (Figure 1b). The Cu–C bond length of 1.781(15) Å, is comparable with other known molecular carbonyl complexes.[44, 66, 67, 72] As per the analogous Cu(I)-ethylene complex, **MnMOF-1**·[Cu(C_2H_4)]BF_4, the charge balancing anion (BF_4^-) occupies a pocket in the MOF pore adjacent to the N,N'-chelated Cu(I) site.

The capacity of anion exchange to generate trigonal planar Cu(I) complexes within **MnMOF-1** led us to explore the use of other anions that are known to be very weakly coordinating.[73] Both hexafluorophosphate (PF_6^-) and triflate (OTf^-) analogues can be prepared via anion exchange in the presence of CO gas, giving **MnMOF-1**·[CuCO]PF_6 and **MnMOF-1**·[CuCO]OTf, respectively. As anticipated **MnMOF-1**·[CuCO]PF_6 and **MnMOF-1**·[CuCO]OTf both show ν(C≡O) stretches close to free CO (2108 cm^{-1} for both complexes). SCXRD studies confirmed a trigonal planar geometry for both complexes (Cu-C = 1.819(16) Å for the OTf derivative; the PF_6 derivative possesses two crystallographically distinct Cu(I) carbonyl sites with 1.782(15) and 1.828(17) Å Cu-C bonds). Again, the respective anions located in a pocket adjacent to the Cu(I) center (Figure 3, note the triflate derivative is very hydroscopic and preventing formation of an aquo complex is extremely challenging, see S6.0 for details). This family of carbonyl complexes further supports the use of *in-situ* anion metathesis as a general method for producing site-isolated, Cu(I) centers possessing highly labile ligands within **MnMOF-1**.

To the best of our knowledge, the only other structurally characterized examples of trigonal planar N,N'-chelated Cu(I) carbonyl complexes have been reported in 2019 by Parasar *et al.*,[67] in 2004 by Dias *et al*.[72] and in 2020 by Huse *et al.*[66] These compounds are supported by polyfluorinated co-ligands based on pyrazolyl, triazapentadienyl or β-diketiminate motifs, producing charge neutral complexes with reduced π-backbonding contributions, as evidenced by high ν(C≡O) stretches (above 2100 cm^{-1}). However, these complexes are unstable, losing coordinated CO if not kept under a CO atmosphere. For comparison, analogous tetrahedral complexes are significantly more stable towards CO loss than the three-coordinate derivatives.[74] Thus, we were interested to explore the stability of the MOF-supported three-coordinate complexes. To this end, storage of **MnMOF-1**·[CuCO]BF_4 in a non-coordinating solvent for several days, under an inert atmosphere, does not result in loss of CO. This difference emphasizes that site isolation in the MOF framework exerts a stabilizing effect on the Cu(I) carbonyl moiety, reducing CO loss.

Motivated by these results, we turned our attention to carrying out simple ligand exchange reactions on the CO and C_2H_4 ligated complexes. **MnMOF-1**·[CuCO]BF_4 crystals were soaked in a non-coordinating solvent under ethylene atmosphere (2 bar). After two days SCXRD was performed and revealed the formation of **MnMOF-1**·[Cu(C_2H_4)]BF_4 indicating that substitution of the carbonyl ligand can be achieved via a SC-SC crystal process. Furthermore, dosing crystals of **MnMOF-1**·[Cu(C_2H_4)]BF_4 with CO (2 bar) lead to formation of **MnMOF-1**·[CuCO]BF_4 (ν(C≡O) stretch at 2105 cm^{-1}) over 48 hours. We then examined the stability of **MnMOF-1**·[Cu(C_2H_4)]BF_4 via gas phase NMR. Samples of **MnMOF-1**·[Cu(C_2H_4)]BF_4 were loaded into an NMR fitted with a Young's tap and were activated at temperatures between 30 °C and 100 °C. After each activation, the tube was dosed with CO and the headspace analyzed via gas phase NMR to determine if ethylene was still present in the complex. The results showed that the ethylene required activation at 100 °C to be removed.

To assess the stability of **MnMOF-1**·[CuCO]BF_4 towards loss of CO, a sample was loaded into an *in situ* FTIR cell (developed in-house, for details see S7.0) connected to a vacuum. During the first 5 minutes, the sample underwent a color change from pale yellow to colorless, with a concomitant diminishing of the CO stretch at 2105 cm^{-1}; after 2 hours evidence of CO bands were absent in the IR (Figure 2). Loss of coordinated CO is accompanied by the temporary appearance of free CO in the FTIR spectra, presumably due to gas being trapped in the MOF pellet; however, the signal quickly dissipates upon gas escape (Figure 2). To determine whether the process is reversible, CO (1 bar) was dosed back into the IR cell. Analysis of the IR data showed that the CO stretch at 2105 cm^{-1} was regenerated (Figure S30), suggesting that the Cu(I) center is stabilized upon CO loss. The *reversible* loss of coordinated CO under vacuum led us to postulate that the anion (BF_4 in this case) binds to, and thereby stabilizes the resulting unsaturated Cu(I) center. We note that in a pertinent report, Fianchini *et al*. characterized the SbF_6 bound complex [Cu(*trans,trans,trans*-1,5,9-cyclododecatriene)(SbF_6)] which features an SbF_6 anion bound by a single fluorine to the Cu(I) center; additionally the anion is readily displaced by CO.[69]

Next, we aimed to structurally characterize **MnMOF-1**·[CuCO]BF_4 following removal of the CO ligand. Crystals of **MnMOF-1**·[CuCO]BF_4 were placed under vacuum for two hours to remove CO, 'backfilled' with dried cyclohexane to protect against moisture and subjected to SCXRD analysis. The crystal structure revealed, as expected from FTIR spectroscopy, an absence of coordinated CO. Furthermore, the charge balancing anion (BF_4) could not be observed in the MOF pore but was instead located in the coordination sphere of the Cu (I) center, albeit disordered over two crystallographically distinct positions (a further two symmetry-generated sites are generated by a mirror plane). This represents a rare example of a Cu(I) complex bearing a coordinated BF_4 anion, of which we are aware of only one other example.[75] Although the formation of this moiety could be posited from the IR spectra, this is an excellent example of how MOFs can be employed as a matrix to facilitate the structural characterization of reactive species via SCXRD.

To assess the porosity of **MnMOF-1**·[Cu(CO)]X (X = BF_4, OTf, PF_6) and **MnMOF-1**·[Cu(C_2H_4)]BF_4 we performed 77 K N_2 gas adsorption isotherms. Activation of **MnMOF-1**·[Cu(CO)]X (X = BF_4, OTf, PF_6) from pentane at room temperature and **MnMOF-1**·[Cu(C_2H_4)]BF_4 from pentane at 100 °C yielded permanently porous materials with BET surface areas of 788, 735, 916 and 754 $m^{2}\cdot g^{-1}$, respectively. We note that these values agree with those observed for other metalated derivatives of **MnMOF-1**. Given the activation conditions employed we anticipate that the CO and ethylene were removed, and that the Cu species consist of anion-bound complexes. In summary, these studies confirm that coordinated CO in **MnMOF-1**·[CuCO]BF_4 is more labile and thus the better 'placeholder' ligand for supported Cu (I) sites in **MnMOF-1**.

Ligand exchange chemistry using MnMOF-1·[CuCO]BF_4

The lability of the CO ligand in **MnMOF-1**·[CuCO]BF_4 encouraged us to explore its ligand exchange chemistry. As discussed earlier, Brookhart and coworkers elegantly employed SCXRD to capture small molecule exchange at a cationic Ir(I) dinitrogen complex in the solid-state (Figure 1).[31] However, in contrast to solid-state molecular crystals; **MnMOF-1** presents a permanently porous matrix within which exchange processes involving larger molecules can be conveniently studied via crystallography. As a proof of principle, **MnMOF-1**·[CuCO]BF_4 was soaked in toluene under an argon atmosphere for 2 days. IR spectroscopy performed on the toluene-soaked samples revealed the disappearance of the CO stretch at 2105 cm^{-1}. SCXRD experiments revealed that the CO had been replaced with a η^2-toluene ligand bound by C2 and C3 of the toluene ring (Figure 3) with the Cu–C bond lengths (Cu-C = 2.146(4), 2.105(4) Å) commensurate with those reported in literature for other Cu η^2-arene complexes.[66, 76-80] Structurally characterized Cu(I) η^2-arene complexes are rare and have been used as precursors for nitrene transfer and Cu(I) borohydride chemistry.[81, 82]

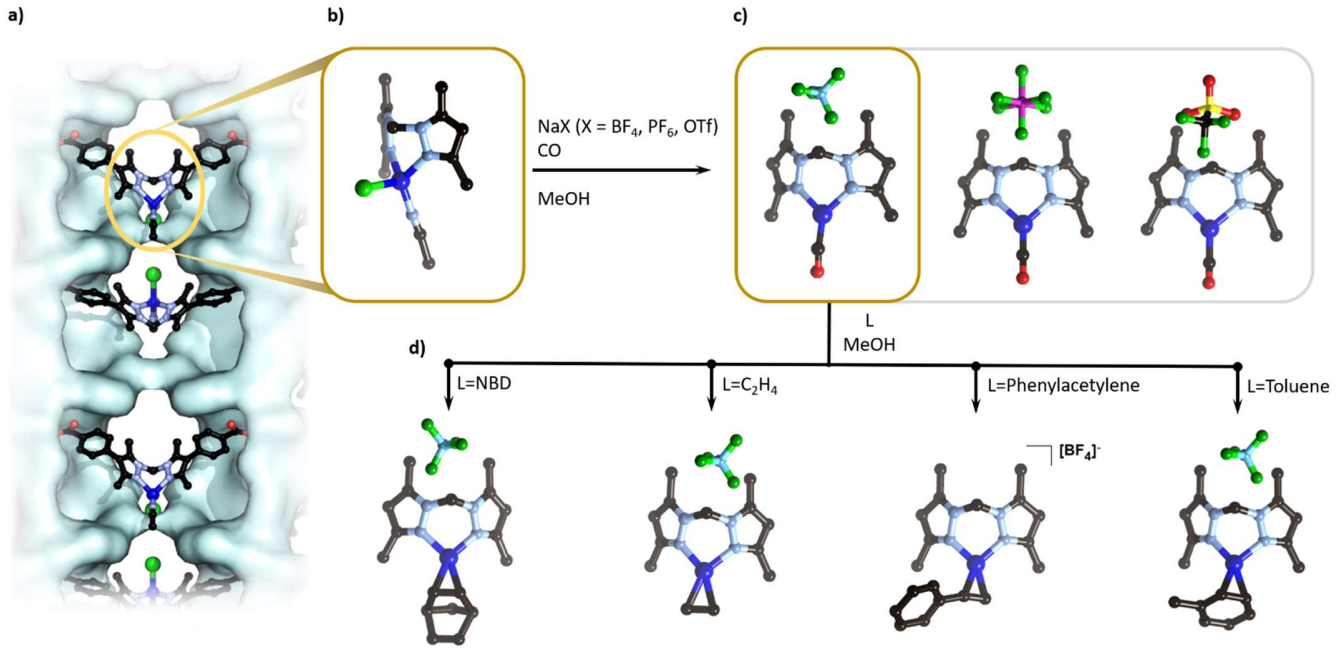

Figure 3. Metalation of **MnMOF-1** with CuCl yields **MnMOF-1**·[CuCl(MeCN)] **(a)** which undergoes quantitative anion exchange **(b)** with NaX (X = BF_4, PF_6, OTf) under an atmosphere of CO to yield the corresponding carbonyl complexes **MnMOF-1**·[CuCO]BF_4, **MnMOF-1**·[CuCO]PF_6 and **MnMOF-1**·[CuCO]OTf **(c)**. **MnMOF-1**·[CuCO]BF_4 undergoes ligand exchange with norbornadiene (NBD), ethylene (C_2H_4), phenylacetylene and toluene to yield the respective π-complexes **(d)**. All carbonyl and π-complexes were structurally characterized after solvent exchange with cyclohexane to ensure clean formation of the trigonal planar derivatives. Hydrogen atoms have been omitted for clarity; the MOF backbone is represented by a blue Van der Waals surface. (C, black; N, lavender; O, red; Cu, blue; B, pale blue; F, green; S, yellow; Cl, lime-green; P, pink).

We further explored the substitution chemistry of CO using other ligands. For example, **MnMOF-1**·[CuCO]BF_4 crystals were soaked in a cyclohexane solution of norbornadiene (NBD) or phenylacetylene (HC≡CPh). In both cases IR spectroscopy confirmed the absence of CO stretches; concurrently SCXRD analysis verified the formation of trigonal planar complexes **MnMOF-1**·[Cu(η^2-NBD)]BF_4 and **MnMOF-**

1·[Cu(η^2-HC≡CPh)]BF_4. **MnMOF-1**·[Cu(η^2-NBD)]BF_4 features a BF_4 counterion in the MOF pore adjacent to the N,N'-chelated Cu(I) site; however, the anion in **MnMOF-1**·[Cu(η^2-HC≡CPh)]BF_4 could not be adequately resolved in the structural model. In the particular case of **MnMOF-1**·[Cu(η^2-NBD)]BF_4, NBD coordinates through only one alkene moiety (Figure 3) with Cu–C distances of 2.026(8) and 2.051(9) Å.[83, 84] In the analogous system, **MnMOF-1**·[Cu(η^2-HC≡CPh)]BF_4, the alkyne coordinates to the Cu(I) center in an η^2-fashion with Cu–C bond lengths of 1.947(14) and 1.88(12) Å.[80, 85] These results emphasize that CO is an excellent 'placeholder' ligand in site-isolated Cu (I) complexes.

Conclusion

Here we showed that ion exchange in the presence of gas molecules facilitates the stabilization of Cu(I) complexes with labile ligands (CO, ethylene) within the porous, crystalline, MOF matrix of **MnMOF-1**. Due to their instability in coordinating solvents and sensitivity to air/moisture, molecular analogues of these complexes are challenging to characterize via SCXRD. We also explored the ligand exchange chemistry of **MnMOF-1**·[CuCO]BF_4 and showed that these SC-SC process could be followed by SCXRD. The inherent characteristics of **MnMOF-1**; high crystallinity, permanent robust porosity, and large pore apertures, renders it an excellent platform to access a broad range of complexes with labile ligands and further, to study ligand substitution processes. We envisage that this chemistry is an important fundamental step towards the synthesis of novel Cu-based species and the exploration of their reactivity within the nanoporous environment of MOF pores.

Experimental

General Considerations

Unless otherwise stated, all chemicals were obtained from commercial sources and used as received. Solvents were dried using literature procedures and degassed with Ar prior to use. Specifically, acetonitrile (MeCN) was dried from CaH_2 under nitrogen; methanol (MeOH) was dried by refluxing them over Mg under N_2; acetone was dried from $CaSO_4$ under nitrogen; and toluene and cyclohexane was dried over Na/benzophenone. $NaBF_4$ used for anion exchange were stored in a 120 ˚C drying oven. The ligand bis-(4-carboxyphenyl-3,5-dimethylpyrazolyl) and **MnMOF-1** were synthesised as previously reported. $[Cu(C_2H_4)_3]SbF_6$ complex was synthesised as reported in the literature.[86] The chemicals carbon monoxide, ethylene, phenylacetylene, norbornadiene and CuCl was obtained from commercial vendors and used without purification. Carbon monoxide is a highly toxic, odorless gas and must be used with extreme caution in a well-ventilated area equipped with a fume cupboard. The high pressure reaction tubes were dosed with CO via a high pressure manifold line and the reaction vessels were stored in a fume cupboard equipped with a CO gas detector at all times.

Powder X-ray diffraction (PXRD) data were collected on a Bruker Advanced D8 diffractometer (capillary stage) using Cu Kα radiation (λ = 1.5456 Å , 40 kW/ 40mA, 2θ = 2 – 52.94°, phi rotation = 20 rotation/min, at 1 sec exposure per step with 5001 steps and using 0.5 mm glass capillaries). Infrared (IR) spectra were collected on a Perkin-Elmer Spectrum Two, with the sample distributed between two NaCl disks in Nujol. Energy dispersive X-ray spectroscopy (EDX) was performed on a Philips XL30 field emission scanning electron microscope. Gas adsorption isotherm measurements were performed on an ASAP 2020 Surface Area and Pore Size Analyzer. Activation of samples was carried out as described.

Preparation of MnMOF-1·[CuClMeCN]

Single crystals of **MnMOF-1** (~24 mg) were placed in a 4 mL glass vial and washed with freshly distilled acetonitrile under Ar flow a total of 5 times (the solution was degassed with Ar after each exchange and the sample was allowed to soak for 1 hr between washings). Under Ar flow, CuCl (30 mg) was added, the vial was sealed under Ar and heated at 4 °C for 3 days. The resulting pale green crystals were washed with freshly distilled acetonitrile five times under Ar flow to give **MnMOF-1**·[Cu(CH_3CN)(Cl). IR ν_{max} (nujol, cm^{-1}): 2289 (w, Cu-N≡CCH_3), 2250 (free, Cu-N≡CCH_3), 1607 (s, C=C), 1550 (m, C=C), 1510 (m, C=C) 1406.

***In situ* anion metathesis to form MnMOF-1·[CuCO]BF_4**

Single crystals of **MnMOF-1**·[Cu(CH_3CN)(Cl)] (~24 mg) were placed in a 20 mL glass pressure vessel fitted with a pressure gauge and Swagelok tap assembly.[12] The crystals were washed with freshly distilled methanol (5 x 5 ml) under Ar flow a total of 5 times (the solution was degassed with Ar after each exchange and the sample was allowed to soak for 1 h between washings). Excess oven dried $NaBF_4$ was added to a small glass ampule which was subsequently submerged in the glass pressure tube containing the MOF sample. The solution was degassed with Ar and the pressure tube was sealed under carbon monoxide (P_T = 4 bar) and allowed them to stand at RT for 3 days. Under argon flow the ampule containing undissolved salt was removed. Finally, the MOF crystals were washed with freshly distilled methanol (5 mL) five times under argon to form **MnMOF-1**·[CuCO]BF_4 as pale-yellow crystals. The samples can be stored under CO atmosphere for 2 weeks. IR ν_{max} (nujol, cm^{-1}): 2105 (m, CO), 1613 (s, C=C), 1549 (m, C=C), 1511 (m, C=C) 1408.

***In-situ* anion metathesis to form MnMOF-1·[Cu(CO)]PF_6 and MnMOF-1·[Cu(CO)]OTf.**

Crystals of **MnMOF-1**·[CuCl(MeCN)] (~24 mg) were placed in a 20 mL glass pressure vessel fitted with a pressure gauge and Swagelok tap assembly.[12] The crystals were washed with freshly distilled MeOH (5 × 5 mL) under Ar flow (the solution was degassed with Ar after each exchange and the sample was allowed to soak for 1 h between washings). A stock solution of dry $NaPF_6$ or NaOTf in distilled MeOH (35 mg, 5 mL) was added to the 20 mL glass tube containing the MOF sample. The solution was degassed with Ar, the pressure tube was sealed under CO atmosphere (PT= 4 bar), and allowed to stand at room temperature for 72 h. Under Ar flow, the ampule containing undissolved salt was removed and the resulting colorless crystals were washed with freshly distilled methanol (5 x 5 mL), acetone (5 x 5 mL) and *n*-pentane (5 x 5 mL). **MnMOF-1**·[Cu(CO)]PF_6 and **MnMOF-1**·[Cu(CO)]OTf can stored under CO atmosphere up to two weeks. **MnMOF-1**·[CuCO]PF_6: IR ν_{max} (nujol, cm^{-1}): 2108 (m, CO), 1615 (s, C=C), 1550 (m, C=C), 1511 (m, C=C) 1408. **MnMOF-1**·[CuCO]OTf: IR ν_{max} (nujol, cm^{-1}): 2108 (m, CO), 1618 (s, C=C), 1552 (m, C=C), 1513 (m, C=C) 1408.

***In-situ* anion metathesis to form MnMOF-1·[Cu(C_2H_4)]BF_4**

Single crystals of MnMOF-1·[Cu(CH_3CN)(Cl)] (~24 mg) were placed in a 20 mL glass pressure vessel fitted with a pressure gauge and Swagelok tap assembly.[12] The crystals were washed with freshly distilled methanol (5 x 5 ml) under Ar flow a total of 5 times (the solution was degassed with Ar after each exchange and the sample was allowed to soak for 1 h between washings). Excess oven dried $NaBF_4$ was added to a small glass ampule which was subsequently submerged in the glass pressure tube containing the MOF sample. The solution was degassed with C_2H_4 and the pressure tube was sealed under ethylene (P_T = 4 bar) and allowed the sample to stand at RT for 3 days. Under ethylene flow **MnMOF-1**·[Cu(C_2H_4)]BF_4 the ampule containing undissolved salt was removed. Finally, the MOF crystals were washed with freshly distilled methanol (5 mL) five times under argon to form **MnMOF-1**·[Cu(C_2H_4)]BF_4 as pale-yellow crystals. The samples can be stored

under ethylene atmosphere for 2 weeks. IR ν_{max} (nujol, cm^{-1}): 1615 (s, C=C), 1549 (m, C=C), 1512 (m, C=C) 1407.

Preparation of MnMOF-1·[Cu(η^2-Toluene)]BF_4

Single crystals of **MnMOF-1**·[CuCO]BF_4 (~24 mg) were placed in a 4 mL glass vial and washed with freshly distilled toluene under Ar flow a total of 5 times (the solution was degassed with Ar after each exchange and the sample was allowed to soak for 1 h between washings). Finally, the vial was sealed under Ar for 2 days to give **MnMOF-1**·[Cu(η^2-Toluene)]BF_4. IR ν_{max} (nujol, cm^{-1}): 1938, 1805, 1797 (m, C=C, toluene), 1616 (s, C=C), 1551 (m, C=C), 1514 (m, C=C) 1413.

Preparation of MnMOF-1·[Cu(η^2-NBD)]BF_4 and MnMOF-1·[Cu(HC≡CPh)]BF_4

Single crystals of **MnMOF-1**·[CuCO]BF_4 (~24 mg) were placed in a 4 ml glass vial and washed with freshly distilled acetone under Ar flow a total of 5 times. Consequently, the crystals were washed with distilled cyclohexane (the solutions were degassed with Ar after each exchange and the sample was allowed to soak for 1 h between washings) five times under argon. Finally, 1 mL of norbonadiene or phenylacetylene were added and the vial was sealed under argon for 2 days to give **MnMOF-1**·[Cu(η^2-NBD)]BF_4 and **MnMOF-1**·[Cu(HC≡CPh)]BF_4 respectively. **MnMOF-1**·[Cu(η^2-NBD)]BF_4: IR ν_{max} (nujol, cm^{-1}): 1619 (s, C=C), 1553 (m, C=C), 1515 (m, C=C) 1415. **MnMOF-1**·[Cu(HC≡CPh)]BF_4: IR ν_{max} (nujol, cm^{-1}): 1936 (w, C≡C), 1622 (s, C=C), 1555 (m, C=C), 1516 (m, C=C) 1416.

Notes

The authors declare no competing financial interest.

Acknowledgements

CJS and CJD gratefully acknowledge the Australian Research Council for funding (DP190101402). This research was undertaken in part using the MX1 and MX2 beamlines at the Australian Synchrotron, part of ANSTO, and made use of the Australian Cancer Research Foundation (ACRF) detector. RAP gratefully acknowledges Adelaide Scholarship International. We acknowledge the contribution of Peter Apoefis in developing the in-situ infra-red spectroscopy cell (S7.0) and high-pressure reaction vessels used in this work.

Supporting Information

Energy Dispersive X-ray Analysis data for all metalated samples (S1.0), Powder X-ray Diffraction plots for each sample (Figures S3-S4), crystal data and refinement parameters of the metalated samples (Tables S2-S4), thermal ellipsoid plots (Figures S5-S14) and electron density maps for each material (Figures S15−S26), 77K N_2 isotherm plots (Figures S27-S29), IR spectra (Figure S30), synthesis of **MnMOF-1**·[Cu(OH_2)]OTf (S6.0) and detailed description of in-situ IR cell (Section 7.0).

References

1. Furukawa, H.; Cordova, K. E.; O'Keeffe, M.; Yaghi, O. M., The chemistry and applications of metal-organic frameworks. *Science* **2013,** *341* (6149), 974-985.
2. Yaghi, O. M.; O'Keeffe, M.; Ockwig, N. W.; Chae, H. K.; Eddaoudi, M.; Kim, J., Reticular synthesis and the design of new materials. *Nature* **2003,** *423* (6941), 705-714.
3. Kitagawa, S.; Kitaura, R.; Noro, S., Functional porous coordination polymers. *Angew. Chem., Int. Ed.* **2004,** *43* (18), 2334-75.
4. Bloch, E. D.; Britt, D.; Lee, C.; Doonan, C. J.; Uribe-Romo, F. J.; Furukawa, H.; Long, J. R.; Yaghi, O. M., Metal Insertion in a Microporous Metal-Organic Framework Lined with 2,2′-Bipyridine. *J. Am. Chem. Soc.* **2010,** *132*, 14382-14384.
5. Gonzalez, M. I.; Bloch, E. D.; Mason, J. A.; Teat, S. J.; Long, J. R., Single-crystal-to-single-crystal metalation of a metal-organic framework: a route toward structurally well-defined catalysts. *Inorg. Chem.* **2015,** *54* (6), 2995-3005.
6. Zhang, T.; Manna, K.; Lin, W., Metal-Organic Frameworks Stabilize Solution-Inaccessible Cobalt Catalysts for Highly Efficient Broad-Scope Organic Transformations. *J. Am. Chem. Soc.* **2016,** *138* (9), 3241-9.
7. Manna, K.; Zhang, T.; Greene, F. X.; Lin, W., Bipyridine- and Phenanthroline-Based Metal–Organic Frameworks for Highly Efficient and Tandem Catalytic Organic Transformations via Directed C–H Activation. *J. Am. Chem. Soc.* **2015,** *137* (7), 2665-2673.

8. Manna, K.; Zhang, T.; Lin, W., Postsynthetic metalation of bipyridyl-containing metal-organic frameworks for highly efficient catalytic organic transformations. *J. Am. Chem. Soc.* **2014,** *136* (18), 6566-9.
9. Morris, W.; Volosskiy, B.; Demir, S.; Gándara, F.; McGrier, P. L.; Furukawa, H.; Cascio, D.; Stoddart, J. F.; Yaghi, O. M., Synthesis, Structure, and Metalation of Two New Highly Porous Zirconium Metal–Organic Frameworks. *Inorg. Chem.* **2012,** *51* (12), 6443-6445.
10. Bloch, W. M.; Burgun, A.; Coghlan, C. J.; Lee, R.; Coote, M. L.; Doonan, C. J.; Sumby, C. J., Capturing snapshots of post-synthetic metallation chemistry in metal-organic frameworks. *Nat. Chem.* **2014,** *6* (10), 906-912.
11. Sun, C.; Skorupskii, G.; Dou, J. H.; Wright, A. M.; Dinca, M., Reversible Metallation and Catalysis with a Scorpionate-like Metallo-ligand in a Metal-Organic Framework. *J. Am. Chem. Soc.* **2018,** *140* (50), 17394-17398.
12. Peralta, R. A.; Huxley, M. T.; Evans, J. D.; Fallon, T.; Cao, H.; He, M.; Zhao, X. S.; Agnoli, S.; Sumby, C. J.; Doonan, C. J., Highly Active Gas Phase Organometallic Catalysis Supported Within Metal-organic Framework Pores. *J. Am. Chem. Soc.* **2020,** *142* (31), 13533-13543.
13. Huxley, M. T.; Burgun, A.; Ghodrati, H.; Coghlan, C. J.; Lemieux, A.; Champness, N. R.; Huang, D. M.; Doonan, C. J.; Sumby, C. J., Protecting-Group-Free Site-Selective Reactions in a Metal-Organic Framework Reaction Vessel. *J. Am. Chem. Soc.* **2018,** *140* (20), 6416-6425.
14. Burgun, A.; Coghlan, C. J.; Huang, D. M.; Chen, W.; Horike, S.; Kitagawa, S.; Alvino, J. F.; Metha, G. F.; Sumby, C. J.; Doonan, C. J., Mapping-Out Catalytic Processes in a Metal-Organic Framework with Single-Crystal X-ray Crystallography. *Angew. Chem., Int. Ed.* **2017,** *56*, 1-6.
15. Dunning, S. G.; Nandra, G.; Conn, A. D.; Chai, W.; Sikma, R. E.; Lee, J. S.; Kunal, P.; Reynolds, J. E., 3rd; Chang, J. S.; Steiner, A.; Henkelman, G.; Humphrey, S. M., A Metal-Organic Framework with Cooperative Phosphines That Permit Post-Synthetic Installation of Open Metal Sites. *Angew. Chem., Int. Ed.* **2018,** *57* (30), 9295-9299.
16. Feng, X.; Song, Y.; Li, Z.; Kaufmann, M.; Pi, Y.; Chen, J. S.; Xu, Z.; Li, Z.; Wang, C.; Lin, W., Metal-Organic Framework Stabilizes a Low-Coordinate Iridium Complex for Catalytic Methane Borylation. *J. Am. Chem. Soc.* **2019,** *141* (28), 11196-11203.
17. Sawano, T.; Lin, Z.; Boures, D.; An, B.; Wang, C.; Lin, W., Metal-Organic Frameworks Stabilize Mono(phosphine)-Metal Complexes for Broad-Scope Catalytic Reactions. *J. Am. Chem. Soc.* **2016,** *138* (31), 9783-6.
18. Evans, J. D.; Sumby, C. J.; Doonan, C. J., Post-synthetic metalation of metal-organic frameworks. *Chem. Soc. Rev.* **2014,** *43* (16), 5933-51.
19. Young, R. J.; Huxley, M. T.; Pardo, E.; Champness, N. R.; Sumby, C. J.; Doonan, C. J., Isolating reactive metal-based species in Metal–Organic Frameworks – viable strategies and opportunities. *Chem. Sci.* **2020,** *11*, 4031-4050.
20. Gonzalez, M. I.; Oktawiec, J.; Long, J. R., Ethylene oligomerization in metal-organic frameworks bearing nickel(II) 2,2'-bipyridine complexes. *Faraday Discuss.* **2017,** *201*, 351-367.
21. Drake, T.; Ji, P.; Lin, W., Site Isolation in Metal–Organic Frameworks Enables Novel Transition Metal Catalysis. *Acc. Chem. Res.* **2018,** *51* (9), 2129-2138.
22. Sikma, R. E.; Kunal, P.; Dunning, S. G.; Reynolds, J. E., 3rd; Lee, J. S.; Chang, J. S.; Humphrey, S. M., Organoarsine Metal-Organic Framework with cis-Diarsine Pockets for the Installation of Uniquely Confined Metal Complexes. *J. Am. Chem. Soc.* **2018,** *140* (31), 9806-9809.

23. Pike, S. D.; Thompson, A. L.; Algarra, A. G.; Apperley, D. C.; Macgregor, S. A.; Weller, A. S., Synthesis and Characterization of a Rhodium(I) σ-Alkane Complex in the Solid State. *Science* **2012,** *337* (6102), 1648-1651.
24. Pike, S. D.; Krämer, T.; Rees, N. H.; Macgregor, S. A.; Weller, A. S., Stoichiometric and Catalytic Solid–Gas Reactivity of Rhodium Bis-phosphine Complexes. *Organometallics* **2015,** *34* (8), 1487-1497.
25. Chadwick, F. M.; Rees, N. H.; Weller, A. S.; Kramer, T.; Iannuzzi, M.; Macgregor, S. A., A Rhodium-Pentane Sigma-Alkane Complex: Characterization in the Solid State by Experimental and Computational Techniques. *Angew. Chem., Int. Ed.* **2016,** *55* (11), 3677-81.
26. Boyd, T. M.; Tegner, B. E.; Tizzard, G. J.; Martinez-Martinez, A. J.; Neale, S. E.; Hayward, M. A.; Coles, S. J.; Macgregor, S. A.; Weller, A. S., A Structurally Characterized Cobalt(I) sigma-Alkane Complex. *Angew. Chem., Int. Ed.* **2020,** *59*, 6177-6181.
27. Ikemoto, K.; Inokuma, Y.; Rissanen, K.; Fujita, M., X-ray Snapshot Observation of Palladium-Mediated Aromatic Bromination in a Porous Complex. *J. Am. Chem. Soc.* **2014,** *136* (19), 6892-6895.
28. Pike, S. D.; Weller, A. S., Organometallic synthesis, reactivity and catalysis in the solid state using well-defined single-site species. *Phil. Trans. R. Soc. A* **2015,** *373* (2037).
29. Chadwick, F. M.; McKay, A. I.; Martinez-Martinez, A. J.; Rees, N. H.; Kramer, T.; Macgregor, S. A.; Weller, A. S., Solid-state molecular organometallic chemistry. Single-crystal to single-crystal reactivity and catalysis with light hydrocarbon substrates. *Chem. Sci.* **2017,** *8* (9), 6014-6029.
30. Albrecht, M.; Lutz, M.; Spek, A. L.; van Koten, G., Organoplatinum crystals for gas-triggered switches. *Nature* **2000,** *406* (6799), 970-974.
31. Huang, Z.; White, P. S.; Brookhart, M., Ligand exchanges and selective catalytic hydrogenation in molecular single crystals. *Nature* **2010,** *465* (7298), 598-601.
32. Huxley, M. T.; Young, R. J.; Bloch, W. M.; Champness, N. R.; Sumby, C. J.; Doonan, C. J., Isomer Interconversion Studied through Single-Crystal to Single-Crystal Transformations in a Metal–Organic Framework Matrix. *Organometallics* **2019,** *38* (18), 3412-3418.
33. Trammell, R.; Rajabimoghadam, K.; Garcia-Bosch, I., Copper-Promoted Functionalization of Organic Molecules: from Biologically Relevant Cu/O2 Model Systems to Organometallic Transformations. *Chemical Reviews* **2019,** *119* (4), 2954-3031.
34. Mohamed, M. H.; Yang, Y.; Li, L.; Zhang, S.; Ruffley, J. P.; Jarvi, A. G.; Saxena, S.; Veser, G.; Johnson, J. K.; Rosi, N. L., Designing Open Metal Sites in Metal–Organic Frameworks for Paraffin/Olefin Separations. *J. Am.Chem. Soc.* **2019,** *141* (33), 13003-13007.
35. Wright, A. M.; Sun, C.; Dincă, M., Thermal Cycling of a MOF-Based NO Disproportionation Catalyst. *J. Am.Chem. Soc.* **2021,** *143* (2), 681-686.
36. Gonzalez, M. I.; Mason, J. A.; Bloch, E. D.; Teat, S. J.; Gagnon, K. J.; Morrison, G. Y.; Queen, W. L.; Long, J. R., Structural characterization of framework-gas interactions in the metal-organic framework Co_2(dobdc) by in situ single-crystal X-ray diffraction. *Chem. Sci.* **2017,** *8* (6), 4387-4398.
37. Runcevski, T.; Kapelewski, M. T.; Torres-Gavosto, R. M.; Tarver, J. D.; Brown, C. M.; Long, J. R., Adsorption of two gas molecules at a single metal site in a metal-organic framework. *Chem. Commun.* **2016,** *52* (53), 8251-4.
38. Bloch, E. D.; Hudson, M. R.; Mason, J. A.; Chavan, S.; Crocella, V.; Howe, J. D.; Lee, K.; Dzubak, A. L.; Queen, W. L.; Zadrozny, J. M.; Geier, S. J.; Lin, L. C.; Gagliardi, L.; Smit, B.; Neaton, J. B.; Bordiga, S.; Brown, C. M.; Long, J. R., Reversible CO binding enables tunable CO/H_2 and CO/N_2 separations in metal-organic frameworks with exposed divalent metal cations. *J. Am. Chem. Soc.* **2014,** *136* (30), 10752-61.

39. Zhang, J.-P.; Liao, P.-Q.; Zhou, H.-L.; Lin, R.-B.; Chen, X.-M., Single-crystal X-ray diffraction studies on structural transformations of porous coordination polymers. *Chem. Soc. Rev.* **2014,** *43* (16), 5789-5814.
40. Easun, T. L.; Moreau, F.; Yan, Y.; Yang, S.; Schröder, M., Structural and dynamic studies of substrate binding in porous metal–organic frameworks. *Chem. Rev.* **2017,** *46* (1), 239-274.
41. van Dijkman, T. F.; Siegler, M. A.; Bouwman, E., Copper(I) Complexes of Naphthyl-Substituted Fluorinated Trispyrazolylborate Ligands with Ethene and Carbon Monoxide. *Eur. J. Inorg. Chem.* **2016,** *2016* (15-16), 2586-2594.
42. Carvajal, M. A.; Novoa, J. J.; Alvarez, S., Choice of Coordination Number in d10 Complexes of Group 11 Metals. *J. Am. Chem. Soc.* **2004,** *126* (5), 1465-1477.
43. Fujisawa, K.; Noguchi, Y.; Miyashita, Y.; Okamoto, K.-i.; Lehnert, N., Mononuclear and Binuclear Copper(I) Complexes Ligated by Bis(3,5-diisopropyl-1-pyrazolyl)methane: Insight into the Fundamental Coordination Chemistry of Three-Coordinate Copper(I) Complexes with a Neutral Coligand. *Inorg. Chem.* **2007,** *46* (25), 10607-10623.
44. Chou, C.-C.; Su, C.-C.; Yeh, A., Mononuclear and Dinuclear Copper(I) Complexes of Bis(3,5-dimethylpyrazol-1-yl)methane: Synthesis, Structure, and Reactivity. *Inorg. Chem.* **2005,** *44* (17), 6122-6128.
45. Adiraju, V. A. K.; Flores, J. A.; Yousufuddin, M.; Dias, H. V. R., Copper(I) Ethylene Complexes Supported by 1,3,5-Triazapentadienyl Ligands with Electron-Withdrawing Groups. *Organometallics* **2012,** *31* (22), 7926-7932.
46. Wang, D.; Jahan, F.; Meise, K. J.; Lindeman, S. V.; Gardinier, J. R., Silver(I) and Copper(I) Complexes of Semi-Bulky Nitrogen-Confused C-Scorpionates. *Eur. J. Inorg. Chem.* **2020,** *2020* (20), 1964-1978.
47. Zelenay, B.; Frutos-Pedreño, R.; Markalain-Barta, J.; Vega-Isa, E.; White, A. J. P.; Díez-González, S., Homo- and Heteroleptic Copper(I) Complexes with Diazabutadiene Ligands: Synthesis, Solution- and Solid-State Structural Studies. *Eur. J. Inorg. Chem.* **2016,** *2016* (28), 4649-4658.
48. Trose, M.; Nahra, F.; Cordes, D. B.; Slawin, A. M. Z.; Cazin, C. S. J., Cu-NHC azide complex: synthesis and reactivity. *Chem Commun* **2019,** *55* (80), 12068-12071.
49. Danopoulos, A. A.; Simler, T.; Braunstein, P., N-Heterocyclic Carbene Complexes of Copper, Nickel, and Cobalt. *Chem. Rev.* **2019,** *119* (6), 3730-3961.
50. Dias, H. V. R.; Wu, J., Structurally Characterized Coinage-Metal–Ethylene Complexes. *Eur. J. Inorg. Chem.* **2008,** *2008* (4), 509-522.
51. Pike, R. D., Structure and Bonding in Copper(I) Carbonyl and Cyanide Complexes. *Organometallics* **2012,** *31* (22), 7647-7660.
52. Díaz-Requejo, M. M.; Pérez, P. J., Coinage Metal Catalyzed C−H Bond Functionalization of Hydrocarbons. *Chem. Rev.* **2008,** *108* (8), 3379-3394.
53. Carsch, K. M.; DiMucci, I. M.; Iovan, D. A.; Li, A.; Zheng, S.-L.; Titus, C. J.; Lee, S. J.; Irwin, K. D.; Nordlund, D.; Lancaster, K. M.; Betley, T. A., Synthesis of a copper-supported triplet nitrene complex pertinent to copper-catalyzed amination. *Science* **2019,** *365* (6458), 1138-1143.
54. Muñoz-Molina, J. M.; Belderrain, T. R.; Pérez, P. J., Trispyrazolylborate coinage metals complexes: Structural features and catalytic transformations. *Coord. Chem. Rev.* **2019,** *390*, 171-189.
55. Dias, H. V. R.; Lu, H.-L.; Kim, H.-J.; Polach, S. A.; Goh, T. K. H. H.; Browning, R. G.; Lovely, C. J., Copper(I) Ethylene Adducts and Aziridination Catalysts Based on Fluorinated Tris(pyrazolyl)borates [HB(3-(CF_3),5-(R)Pz)$_3$]- (where R = CF_3, C_6H_5, H; Pz = pyrazolyl). *Organometallics* **2002,** *21* (7), 1466-1473.
56. Flores, J. A.; Dias, H. V. R., Gold(I) Ethylene and Copper(I) Ethylene Complexes Supported by a Polyhalogenated Triazapentadienyl Ligand. *Inorg. Chem.* **2008,** *47* (11), 4448-4450.

57. Flores, J. A.; Badarinarayana, V.; Singh, S.; Lovely, C. J.; Dias, H. V. R., Synthesis and catalytic activity of an electron-deficient copper–ethylene triazapentadienyl complex. *Dalton Trans.* **2009,** (37), 7648-7652.
58. Gustafsson, B.; Håkansson, M.; Jagner, S., Complexes between copper(I) chloride and polydentate aromatic amines. *Inorganica Chim. Acta* **2003,** *350*, 209-214.
59. Cowieson, N. P.; Aragao, D.; Clift, M.; Ericsson, D. J.; Gee, C.; Harrop, S. J.; Mudie, N.; Panjikar, S.; Price, J. R.; Riboldi-Tunnicliffe, A.; Williamson, R.; Caradoc-Davies, T., MX1: a bending-magnet crystallography beamline serving both chemical and macromolecular crystallography communities at the Australian Synchrotron. *J. Synchrotron Radiat.* **2015,** *22* (1), 187-190.
60. Aragao, D.; Aishima, J.; Cherukuvada, H.; Clarken, R.; Clift, M.; Cowieson, N. P.; Ericsson, D. J.; Gee, C. L.; Macedo, S.; Mudie, N.; Panjikar, S.; Price, J. R.; Riboldi-Tunnicliffe, A.; Rostan, R.; Williamson, R.; Caradoc-Davies, T. T., MX2: a high-flux undulator microfocus beamline serving both the chemical and macromolecular crystallography communities at the Australian Synchrotron. *J. Synchrotron Rad.* **2018,** *25* (3), 885-891.
61. Ridlen, S. G.; Kulkarni, N. V.; Dias, H. V. R., Monoanionic, Bis(pyrazolyl)methylborate [(Ph_3B)CH(3,5-(CH_3)$_2$Pz)$_2$)](-) as a Supporting Ligand for Copper(I)-ethylene, cis-2-Butene, and Carbonyl Complexes. *Inorg. Chem.* **2017,** *56* (12), 7237-7246.
62. Dias, H. V. R.; Lovely, C. J., Carbonyl and Olefin Adducts of Coinage Metals Supported by Poly(pyrazolyl)borate and Poly(pyrazolyl)alkane Ligands and Silver Mediated Atom Transfer Reactions. *Chem. Rev.* **2008,** *108* (8), 3223-3238.
63. Peralta, R.; Huxley, M.; Young, R.; Linder-Patton, O. M.; Evans, J. D.; Doonan, C. J.; Sumby, C. J., MOF Matrix Isolation: Cooperative Conformational Mobility Enables Reliable Single Crystal Transformations. *Faraday Discuss.* **2020,** *225*, 84-99.
64. Masuda, H. Y., N.; Taga, T.; Machida, K., Structural Studies of Copper(I) complexes with ethylene. Crystal Structures of [Cu(2,2'-bipyradine)(ethylene)]ClO_4, and [Cu(1,10-phenanthroline)(ethylene)]ClO_4 *J. Organomet. Chem.* **1987,** *322*, 121-129.
65. Klimovica, K.; Kirschbaum, K.; Daugulis, O., Synthesis and Properties of "Sandwich" Diimine-Coinage Metal Ethylene Complexes. *Organometallics* **2016,** *35* (17), 2938-2943.
66. Huse, K.; Weinert, H.; Wölper, C.; Schulz, S., Electronic effect of a perfluorinated β-diketiminate ligand on the bonding nature of copper carbonyl complexes. *Dalton Trans.* **2020,** *49* (28), 9773-9780.
67. Parasar, D.; Jayaratna, N. B.; Muñoz-Castro, A.; Conway, A. E.; Mykhailiuk, P. K.; Dias, H. V. R., Carbonyl complexes of copper(i) stabilized by bridging fluorinated pyrazolates and halide ions. *Dalton Trans.* **2019,** *48* (19), 6358-6371.
68. Bruce, M. I.; Ostazewski, A. P. P., Group IB metal chemistry. Part I. Preparation and reactions of the carbonyl(hydrotripyrazol-1-ylborato)copper(I) complex. *Dalt. Trans.* **1973,** (22), 2433-2436.
69. Fianchini, M.; Cundari, T. R.; DeYonker, N. J.; Dias, H. V. R., A non-classical copper carbonyl on a tri-alkene hydrocarbon support. *Dalton Trans.* **2009,** (12), 2085-2087.
70. Ivanova, S. M.; Ivanov, S. V.; Miller, S. M.; Anderson, O. P.; Solntsev, K. A.; Strauss, S. H., Mono-, Di-, Tri-, and Tetracarbonyls of Copper(I), Including the Structures of $Cu(CO)_2$(1-Bn-$CB_{11}F_{11}$) and [$Cu(CO)_4$][1-Et-$CB_{11}F_{11}$]. *Inorg. Chem.* **1999,** *38* (17), 3756-3757.
71. Papish, E. T.; Donahue, T. M.; Wells, K. R.; Yap, G. P. A., How are tris(triazolyl)borate ligands electronically different from tris(pyrazolyl)borate ligands? A study of (TtztBu,Me)CuCO [TtztBu,Me = tris(3-t-butyl-5-methyl-1,2,4-triazolyl)borate]. *Dalton Trans.* **2008,** (22), 2923-2925.

72. Dias, H. V. R.; Singh, S., Copper(I) Complexes of Fluorinated Triazapentadienyl Ligands: Synthesis and Characterization of [N{(C_3F_7)C(Dipp)N}$_2$]CuL (Where L = $NCCH_3$, CNBut, CO; Dipp = 2,6-Diisopropylphenyl). *Inorg. Chem.* **2004,** *43* (19), 5786-5788.
73. Strauss, S. H., The search for larger and more weakly coordinating anions. *Chem. Rev.* **1993,** *93* (3), 927-942.
74. Pampaloni, G.; Peloso, R.; Belletti, D.; Graiff, C.; Tiripicchio, A., Trifluoromethyl-Substituted Bis(pyrazolyl)methanes as Ligands for Copper and Silver: Synthesis and Spectroscopic and Structural Characterization. *Organometallics* **2007,** *26* (17), 4278-4286.
75. Gandhi, B. A.; Green, O.; Burstyn, J. N., Facile Oxidation-Based Synthesis of Sterically Encumbered Four-Coordinate Bis(2,9-di-tert-butyl-1,10-phenanthroline)copper(I) and Related Three-Coordinate Copper(I) Complexes. *Inorg. Chem.* **2007,** *46* (10), 3816-3825.
76. Parvin, N.; Hossain, J.; George, A.; Parameswaran, P.; Khan, S., N-heterocyclic silylene stabilized monocordinated copper(i)–arene cationic complexes and their application in click chemistry. *Chem. Commun.* **2020,** *56* (2), 273-276.
77. Dines, M. B.; Bird, P. H., Aromatic complexes of copper(I) trifluoromethanesulphonate. *Chem. Commun.* **1973,** (1), 12-12.
78. R. Conry, R., Synthesis of copper(I) complexes with a novel naphthyl-appended macrocyclic ligand, including the crystal and molecular structure of the first copper(I)–η^2-naphthyl complex. *Chem. Commun.* **1998,** (5), 555-556.
79. Lee, S. Y.; Na, S. J.; Kwon, H. Y.; Lee, B. Y.; Kang, S. O., Syntheses and Structures of a Macrocyclic β-Diketimine and Its Zinc and Copper Complexes. *Organometallics* **2004,** *23* (23), 5382-5385.
80. Badiei, Y. M.; Warren, T. H., Electronic structure and electrophilic reactivity of discrete copper diphenylcarbenes. *J. Organomet. Chem.* **2005,** *690* (24), 5989-6000.
81. Badiei, Y. M.; Dinescu, A.; Dai, X.; Palomino, R. M.; Heinemann, F. W.; Cundari, T. R.; Warren, T. H., Copper-nitrene complexes in catalytic C-H amination. *Angew. Chem., Int. Ed.* **2008,** *47* (51), 9961-4.
82. Nako, A. E.; White, A. J.; Crimmin, M. R., Bis(sigma-B-H) complexes of copper(i): precursors to a heterogeneous amine-borane dehydrogenation catalyst. *Dalton Trans.* **2015,** *44* (28), 12530-4.
83. Speier, G.; Szabó, L.; Fülöp, V., Preparation and molecular structure of an adipinato copper norbornadiene complex. *J. Organomet. Chem.* **1993,** *462* (1), 375-378.
84. Stricker, M.; Oelkers, B.; Rosenau, C. P.; Sundermeyer, J., Copper(I) and Silver(I) Bis(trifluoromethanesulfonyl)imide and Their Interaction with an Arene, Diverse Olefins, and an NTf^2–-Based Ionic Liquid. *Chem. Eur. J.* **2013,** *19* (3), 1042-1057.
85. Dias, H. V. R.; Flores, J. A.; Wu, J.; Kroll, P., Monomeric Copper(I), Silver(I), and Gold(I) Alkyne Complexes and the Coinage Metal Family Group Trends. *J. Am. Chem. Soc.* **2009,** *131* (31), 11249-11255.
86. Fianchini, M.; Campana, C. F.; Chilukuri, B.; Cundari, T. R.; Petricek, V.; Dias, H. V. R., Use of $[SbF_6]^-$ to Isolate Cationic Copper and Silver Adducts with More than One Ethylene on the Metal Center. *Organometallics* **2013,** *32* (10), 3034-3041.

Table of contents graphic:

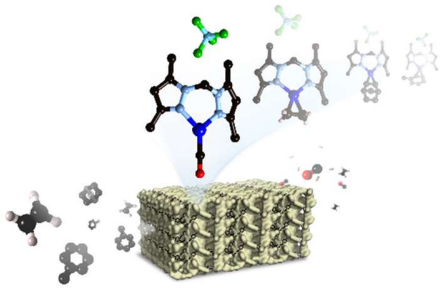

Synopsis

Due to unwanted dinucleation or ligand substitution reactions, transition metal complexes bearing labile ligands can be difficult to isolate and study in solution. Herein we report the development of an *in-situ* anion metathesis strategy which facilitates the post-synthetic modification of Cu(I) complexes appended to a porous, crystalline Metal-organic Framework (MOF). This enables a series of labile MOF-appended Cu(I) complexes featuring carbon monoxide or ethylene ligands to be prepared and structurally characterized using X-ray crystallography.

Supplementary Information for

Single-crystal to Single-crystal transformations of MOF-supported, site-isolated trigonal planar Cu(I) complexes with labile ligands

Ricardo A. Peralta[a], Michael T. Huxley[a], Jorge Albalad[a], Christopher J. Sumby[a]* and Christian J. Doonan[a]*

[a] Centre for Advanced Nanomaterials and Department of Chemistry, The University of Adelaide, North Terrace, Adelaide, SA 5000, Australia. Email: christopher.sumby@adelaide.edu.au (CJS); christian.doonan@adelaide.edu.au (CJD)

Contents

S1.0 Energy Dispersive X-ray (EDX) analysis

Table S1: Cu(I) and associated anion occupancy determined via measurement of the Mn:Cu ratio and the Cu:Cl ratio using EDX analysis.

Sample	Cu, occupancy (%)[a,b]	Cl occupancy (%)[a,b]	Std error (%)
MnMOF-1·[Cu(CH_3CN)(Cl)]	101.5	110.3	7.6
MnMOF-1·[Cu(C_2H_4)]BF_4	102.3	0.8	1.2
MnMOF-1·[CuCO]BF_4	106.2	0.2	3.5
MnMOF-1·[CuCO]PF_6	104.2	0.5	4.1
MnMOF-1·[CuCO]OTf	99.7	0.4	3.9

[a] Average atomic% obtained from three areas of crystals.
[b] Relative to full occupancy of the bis(pyrazole)methane coordinating sites in **1**.

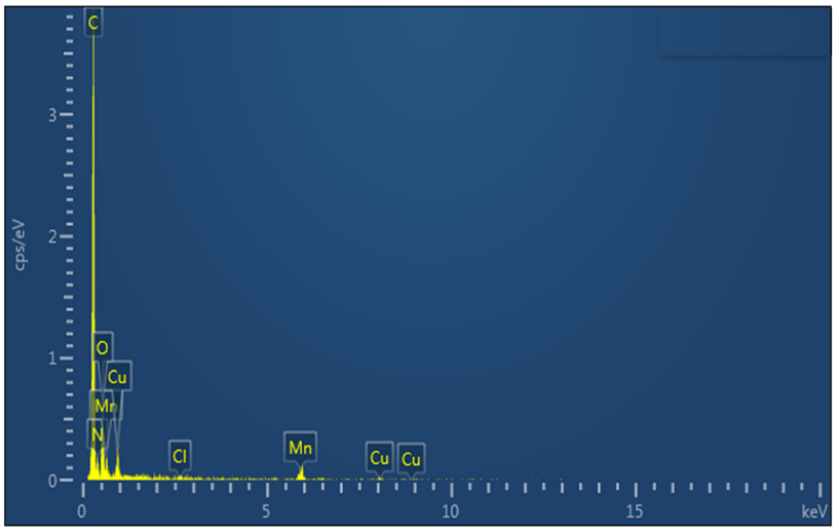

Figure S1: Representative raw EDX spectra for **MnMOF-1**·[Cu(CH_3CN)(Cl).

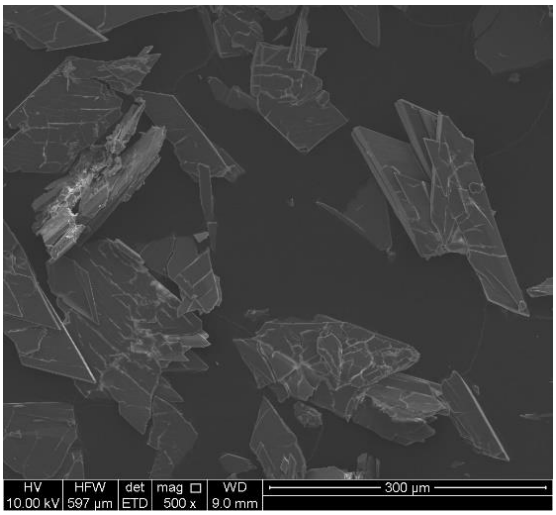

Figure S2: SEM image of metalated **MnMOF-1** showing an area of crushed crystals used for EDX analysis.

S2.0 Powder X-ray Diffraction (PXRD) plots

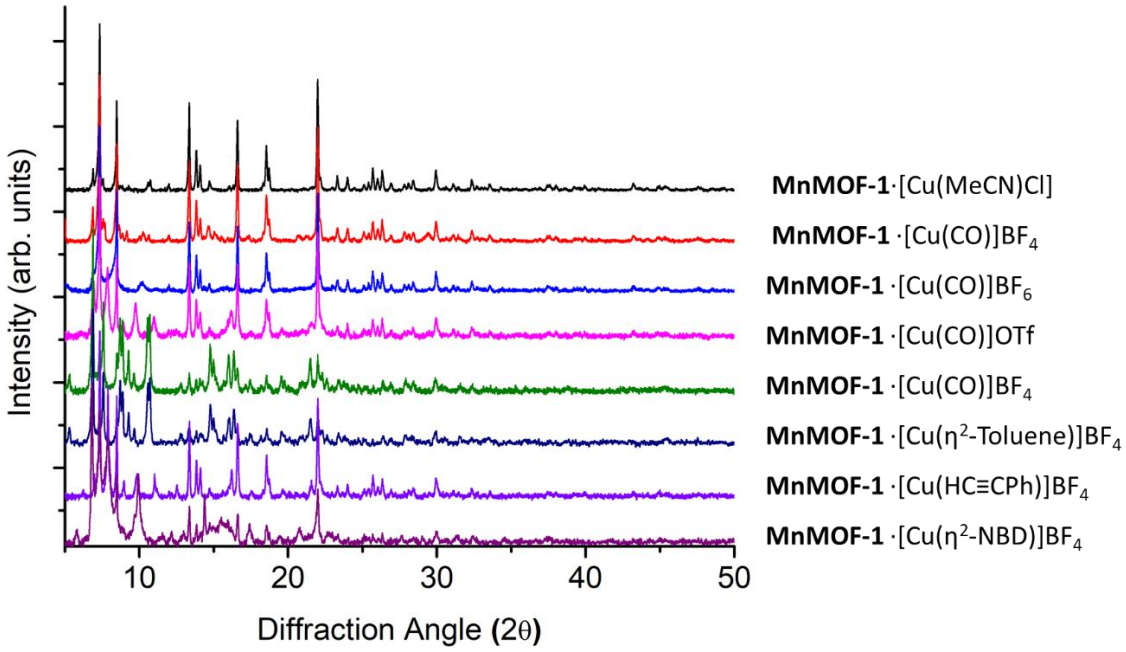

Figure S3: Experimental PXRD plots for **MnMOF-1**·[Cu(MeCN)Cl], **MnMOF-1**·[Cu(CO)]BF_4, **MnMOF-1**·[Cu(CO)]PF_6, **MnMOF-1**·[Cu(CO)]OTf, **MnMOF-1**·[Cu(C_2H_4)]PF_6, **MnMOF-1**·[Cu(η^2-Toluene)]BF_4, **MnMOF-1**·[Cu(HC≡CPh)]BF_4 and **MnMOF-1**·[Cu(η^2-NBD)]BF_4. The flexibility of the framework causes slight shifts in the PXRD peak positions and intensity upon changes in the solvent and loss of solvent during sample preparation for PXRD.

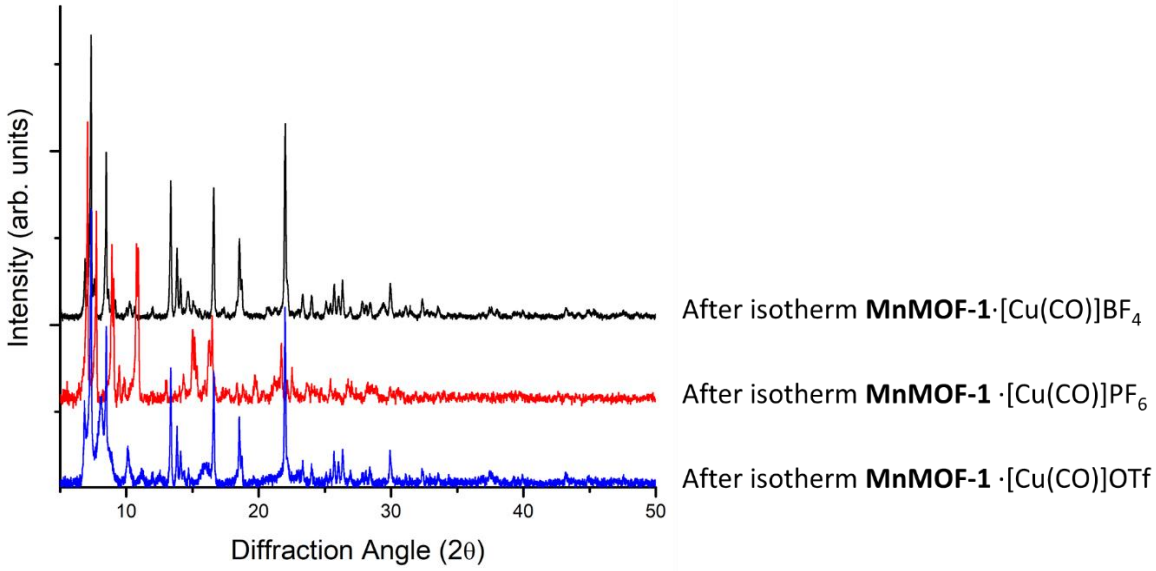

Figure S4: Experimental PXRD plots after the isotherms for **MnMOF-1**·[Cu(CO)]BF_4, **MnMOF-1**·[Cu(CO)]OTf, and **MnMOF-1**·[Cu(CO)]PF_6. The flexibility of the framework causes slight shifts in the PXRD peak positions and intensity upon changes in the solvent and loss of solvent during activation and/or sample preparation for PXRD.

S3.0 Single Crystal X-ray Crystallography

S3.1 General Procedures

Single crystals were mounted in Paratone-N oil on a MiTeGen micromount. Single-crystal X-ray data were collected at 100 K on the MX1 or MX2 beamlines of the Australian Synchrotron using the Blue-ice software interface,[1] λ = 0.71073 Å. Absorption corrections were applied using multiscan methods using XDS,[2, 3] the structures solved using SHELXS or SHELXT,[4, 5] and refined by full-matrix least squares on F^2 by SHELXL,[6] interfaced through the program X-Seed or OLEX.[7, 8] In general, all atoms were refined anisotropically and hydrogens atoms were included as invariants at geometrically estimated positions, unless specified otherwise in additional details in supporting information. Where noted, the data was treated with the SQUEEZE routine available in Platon[9] or using the solvent masking feature of Olex. Figures were produced using the program CrystalMaker. X-ray experimental data is given in Tables S2 – S4. CIF data have been deposited with the Cambridge Crystallographic Data Centre, CCDC reference numbers CCDC 2071194-2071203.

The structures reported in this manuscript are all metal-organic framework structures whose crystals:

- are prepared in multi-step crystal-to-crystal reaction sequences involving numerous solvent washing steps, chemical reactions and anion exchanges;
- are weakly diffracting (all data collections reported were obtained at a synchrotron facility, including in some cases on an undulator based beamline, which provides additional flux);
- have a binding site that has the capacity to be disordered (and typically shows a small contribution of a disorder site in most of the reported structures); and,
- has significant diffuse scattering from solvent, anions, and other guests in the pore network.

These factors all create challenges for the structure determination and are shown by a handful of level A/B alerts registered by standard checking software. In addition, standard measures of refinement, such as R_1, wR_2 and GooF can be higher than typical crystals of close-packed inorganic structures, which can flag additional alerts. All A-level alerts are addressed in the cifs that are submitted and most level B-alerts relate to similar issues with the data collection, data quality or structural models and hence were not explicitly noted.

S3.2 Specific Refinement Details

MnMOF-1·[Cu(CH_3CN)(Cl)]. The coordination environment of the added [Cu(CH_3CN)(Cl)] moieties (two independent positions with different coordination environments) is significantly disordered. A series of SIMU, RIGU, and ISOR restrains were used to allow refinement.

MnMOF-1·[CuCO]BF_4. SIMU, RIGU and DFIX restraints were used to refine the Cu-CO moiety with chemically sensible bond lengths.

MnMOF-1·[CuCO]PF_6. SIMU, RIGU and DFIX restraints were used to refine the Cu-CO moiety with chemically sensible bond lengths. Additionally, SIMU and RIGU restraints were used stabilising the refinement and attaining chemically sensible ellipsoids for the organic linkers of the MOF.

MnMOF-1·[CuCO]OTf. SIMU, RIGU and DFIX restraints were used to refine the Cu-CO moiety with chemically sensible bond lengths. A significant proportion of the Cu centres had undergone hydrolysis to form [Cu(OH_2)]; this was approximately 50:50 in one instance and mainly the [Cu(OH_2)] complex rather than the target [CuCO]OTf species in the other crystallographically independent site. SIMU, RIGU, DFIX and ISOR restraints were also used to allow refinement of the cyclohexane solvate molecules.

MnMOF-1·[Cu(C_2H_4)]BF_4. SIMU, RIGU, ISOR and DFIX restraints were used to refine the Cu-(C_2H_4) moiety with chemically sensible bond lengths. Additional ISOR restraints were used for the fluorine atoms of the tetrafluoroborate anion.

MnMOF-1·[$CuBF_4$]. The BF_4 anion is disordered over four positions in the structure; two crystallographically independent sites and two sites generated by a mirror plane. Due to the relatively low occupancy in each site (0.25) a model of the BF_4 anion from the FragmentDB library was used to allow isotropic refinement (DFIX, SADI restraints). SIMU and RIGU restraints were also used for the Cu(BF_4) moiety and parts of the organic linkers of the MOF (rotational disorder). There was a small amount of residual CuCO moiety from the starting material present in the sample (**MnMOF-1**·[$CuBF_4$] was formed by evacuating **MnMOF-1**·[CuCO]BF_4 and resolvating the crystals), but this could not be modelled.

MnMOF-1·[Cu(η^2-Toluene)]BF_4. DFIX, SIMU, RIGU and ISOR restraints were used to allow the refinement of the toluene solvate molecules.

MnMOF-1 ·[Cu(η^2-NBD)]BF_4. DFIX, SIMU, RIGU and ISOR restraints were used to allow the refinement of the coordinated norbornadiene (NBD), tetrafluoroborate anion, and toluene solvate molecules.

MnMOF-1 ·[Cu(η^2(HC≡CPh)]BF_4. A large series of restraints (FLAT, SIMU, RIGU, EADP, ISOR and DFIX) were used to allow the refinement of the coordinated phenylacetylene (PhCCH), organic linkers, and phenylacetylene solvate molecules. The non-coordinated phenylacetylene molecules were also refined with isotropic displacement parameters (ca. 50% occupied). Finally, due to disorder, the tetrafluoroborate anion could not be located in the structure, although a possible site in the known anion pocket was identified.

S3.3 Thermal ellipsoid plots for all structures at the 50% probability level

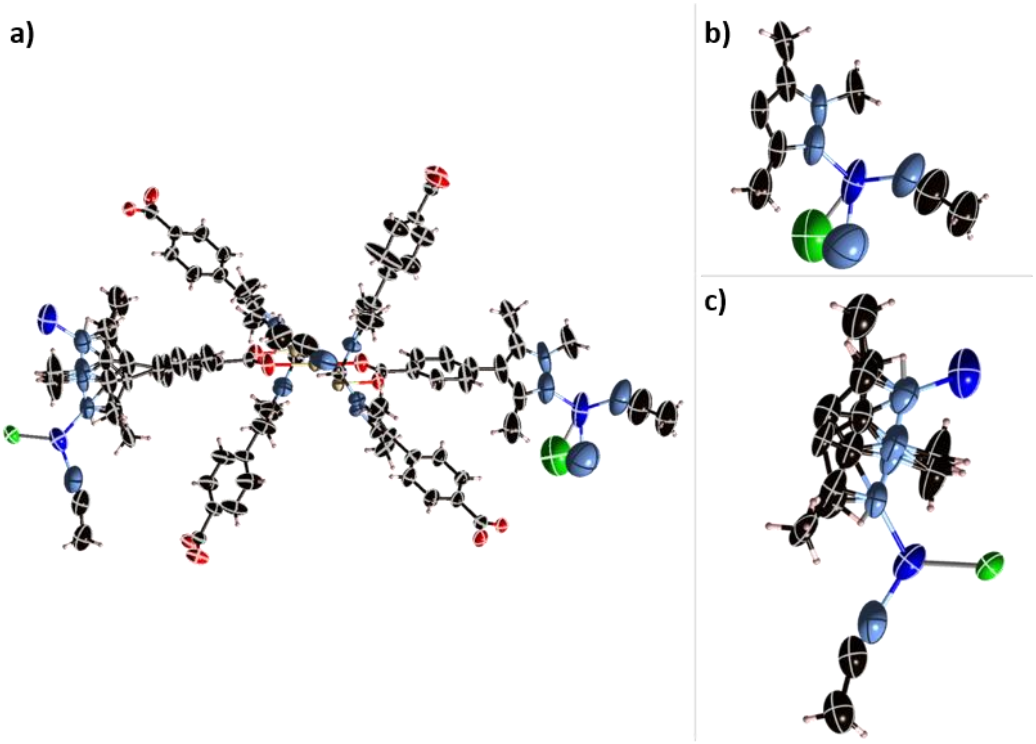

Figure S5: (a) The asymmetric unit of **MnMOF-1**·[Cu(CH_3CN)(Cl)], with all non-hydrogen atoms represented by ellipsoids at the 50% probability level (C, black; H, white; N, light blue; O, red; Cu, dark blue; Mn, beige; Cl, green). (b) and (c) present perspective views of the crystallographically distinct Cu(I) chelation sites with all non-hydrogen atoms represented by ellipsoids at the 50% probability level.

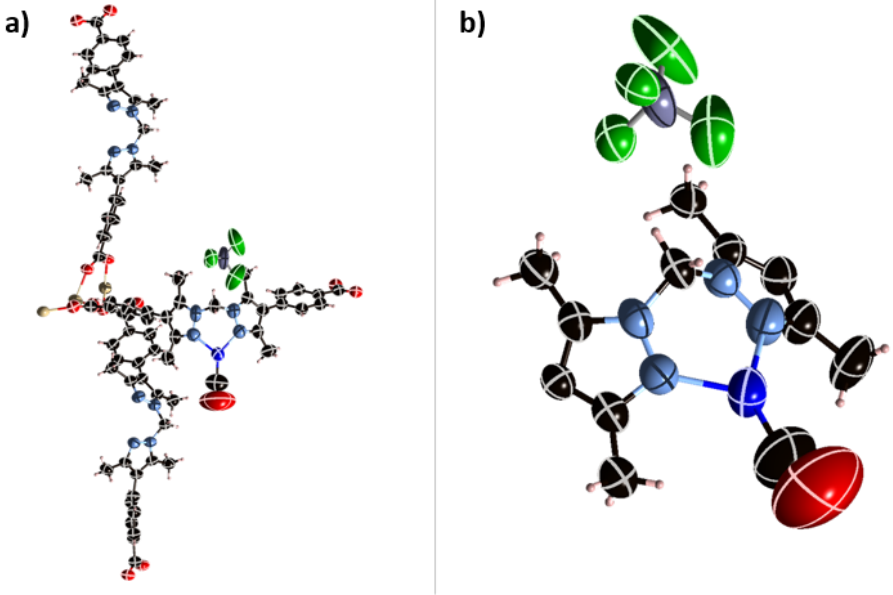

Figure S6: (a) The asymmetric unit of **MnMOF-1**·[CuCO]BF_4, with all non-hydrogen atoms represented by ellipsoids at the 50% probability level (C, black; H, white; N, light blue; O, red; Cu, dark blue; Mn, beige; B, grey; F, green). (b) A perspective view of the Cu(I) chelation site with all non-hydrogen atoms represented by ellipsoids at the 50% probability level.

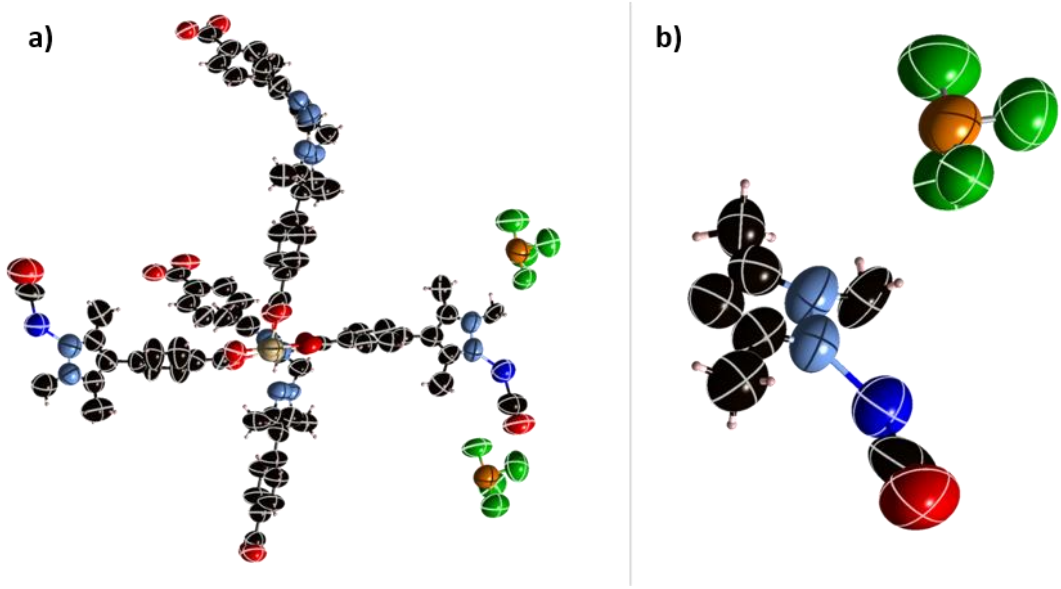

Figure S7: (a) The asymmetric unit of **MnMOF-1**·[CuCO]PF_6, with all non-hydrogen atoms represented by ellipsoids at the 50% probability level (C, black; H, white; N, light blue; O, red; Cu, dark blue; Mn, beige; P, orange; F, green). (b) A perspective view of the Cu(I) chelation site with all non-hydrogen atoms represented by ellipsoids at the 50% probability level.

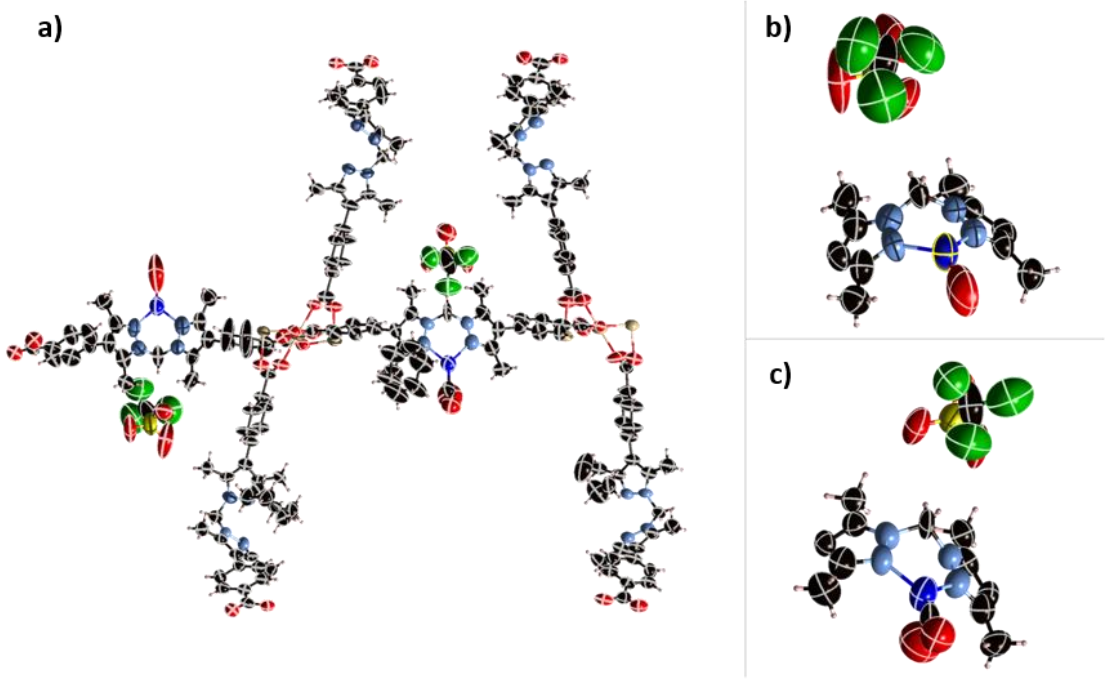

Figure S8: (a) The asymmetric unit of **MnMOF-1**·[CuCO]OTf, with all non-hydrogen atoms represented by ellipsoids at the 50% probability level (C, black; H, white; N, light blue; O, red; Cu, dark blue; Mn, beige; S, yellow; F, green). (b) and (c) present perspective views of the two Cu(I) chelation site with all non-hydrogen atoms represented by ellipsoids at the 50% probability level.

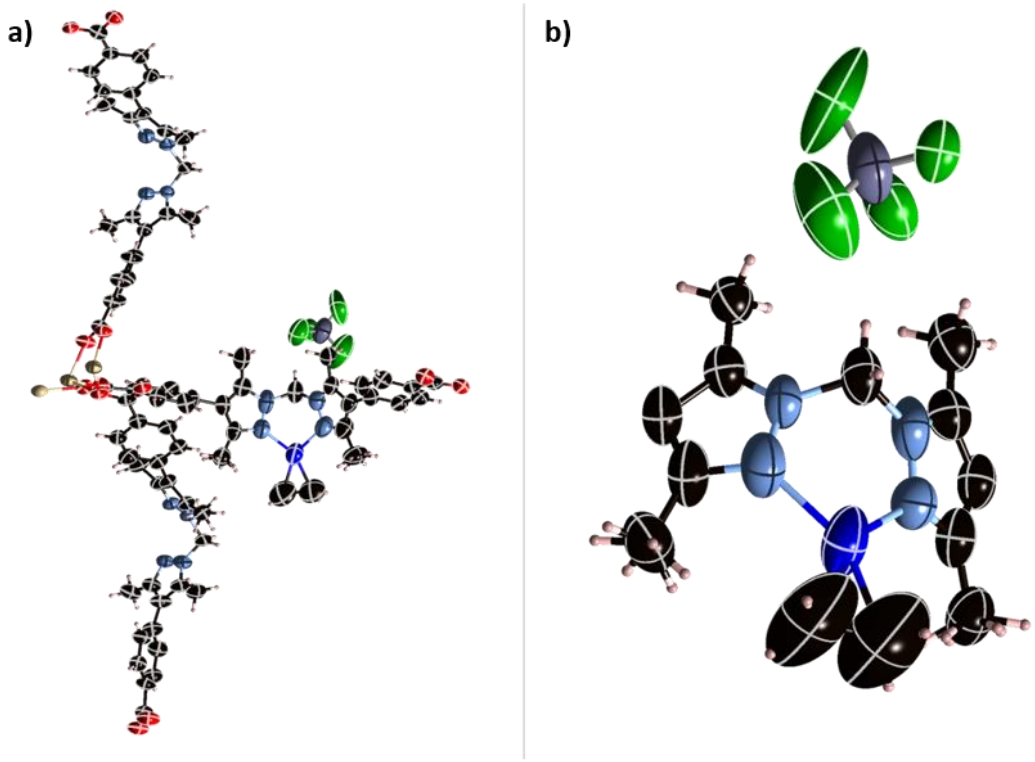

Figure S9: (a) The asymmetric unit of **MnMOF-1**·[Cu(C_2H_4)]BF_4, with all non-hydrogen atoms represented by ellipsoids at the 50% probability level (C, black; H, white; N, light blue; O, red; Cu, dark blue; Mn, beige; B, grey; F, green). (b) A perspective view of the Cu(I) chelation site with all non-hydrogen atoms represented by ellipsoids at the 50% probability level.

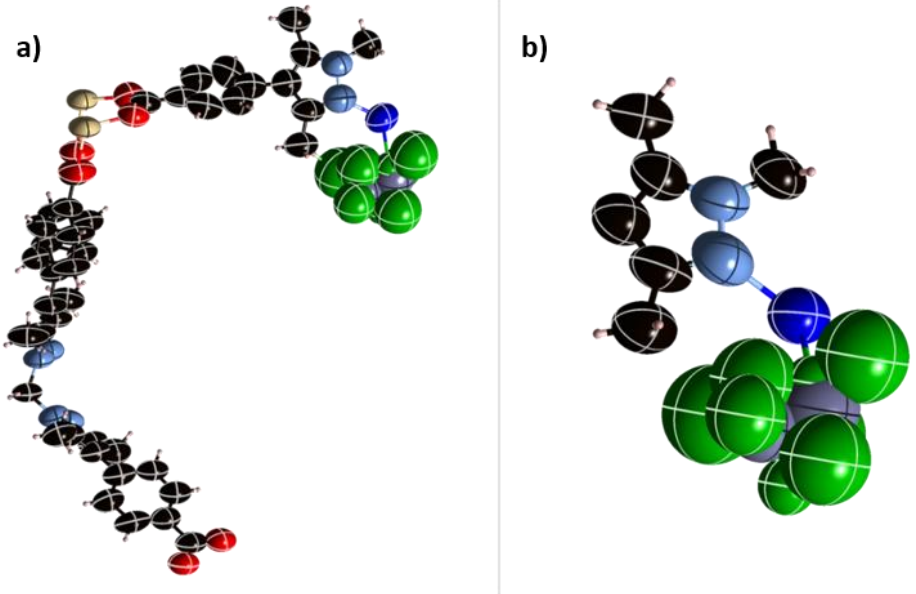

Figure S10: (a) The asymmetric unit of **MnMOF-1**·[$CuBF_4$], with all non-hydrogen atoms represented by ellipsoids at the 50% probability level (C, black; H, white; N, light blue; O, red; Cu, dark blue; Mn, beige; B, grey; F, green). (b) A perspective view of the Cu(I) chelation site with all non-hydrogen atoms, except the disordered tetrafluoroborate anion represented by ellipsoids at the 50% probability level.

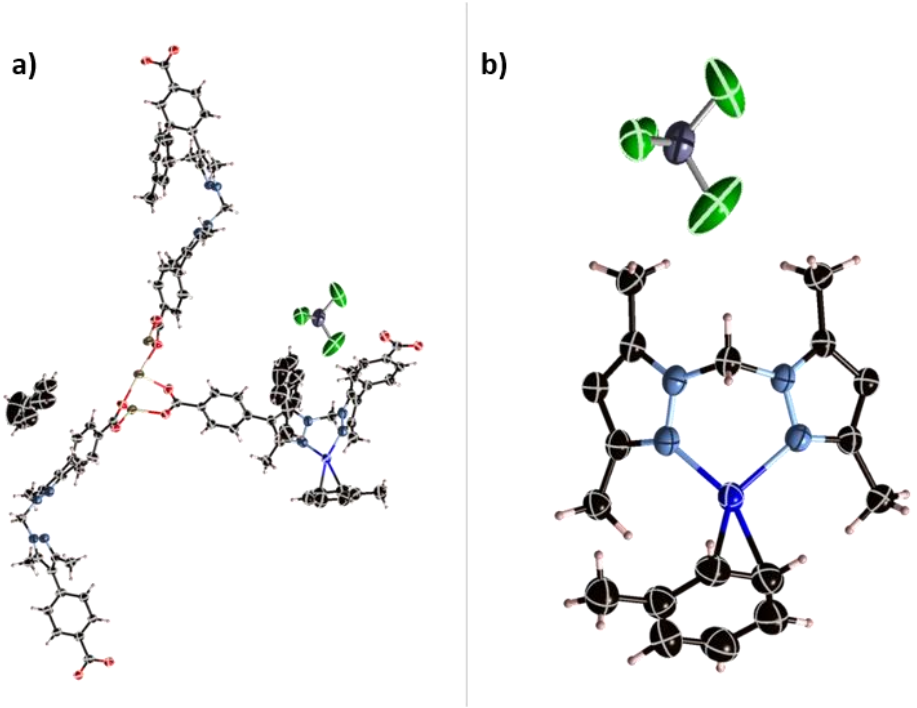

Figure S11: (a) The asymmetric unit of **MnMOF-1**·[Cu(η^2-Toluene)]BF_4 with all non-hydrogen atoms represented by ellipsoids at the 50% probability level (C, black; H, white; N, light blue; O, red; Cu, dark blue; Mn, beige; B, grey; F, green). (b) A perspective view of the Cu(I) chelation site with all non-hydrogen atoms represented by ellipsoids at the 50% probability level.

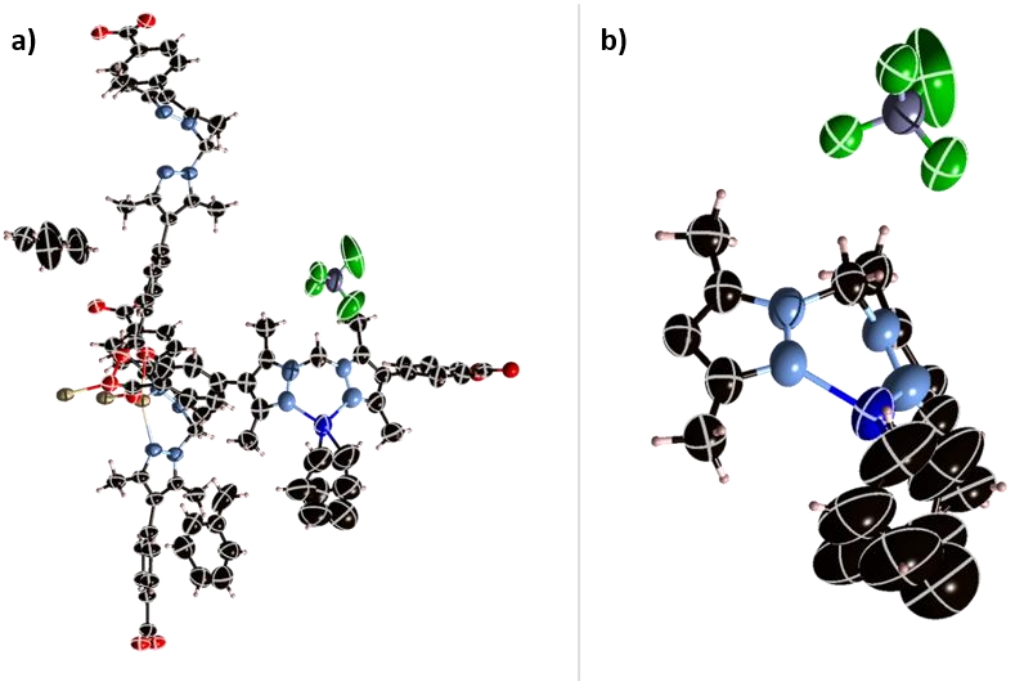

Figure S12: (a) The asymmetric unit of **MnMOF-1** [Cu(η^2-NBD)]BF_4 with all non-hydrogen atoms represented by ellipsoids at the 50% probability level (C, black; H, white; N, light blue; O, red; Cu, dark blue; Mn, beige; B, grey; F, green). (b) A perspective view of the Cu(I) chelation site with all non-hydrogen atoms represented by ellipsoids at the 50% probability level.

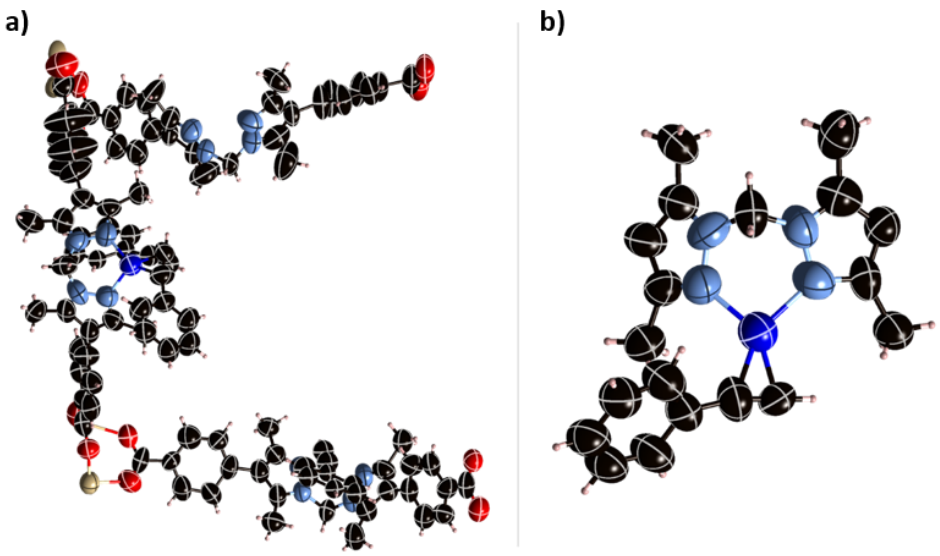

Figure S13: (a) The asymmetric unit of **MnMOF-1** [Cu(η^2(HC≡CPh)]BF_4 with all non-hydrogen atoms represented by ellipsoids at the 50% probability level (C, black; H, white; N, light blue; O, red; Cu, dark blue; Mn, beige). (b) A perspective view of the Cu(I) chelation site with all non-hydrogen atoms represented by ellipsoids at the 50% probability level. The tetrafluoroborate anion required for charge balance could not be satisfactorily modelled due to disorder.

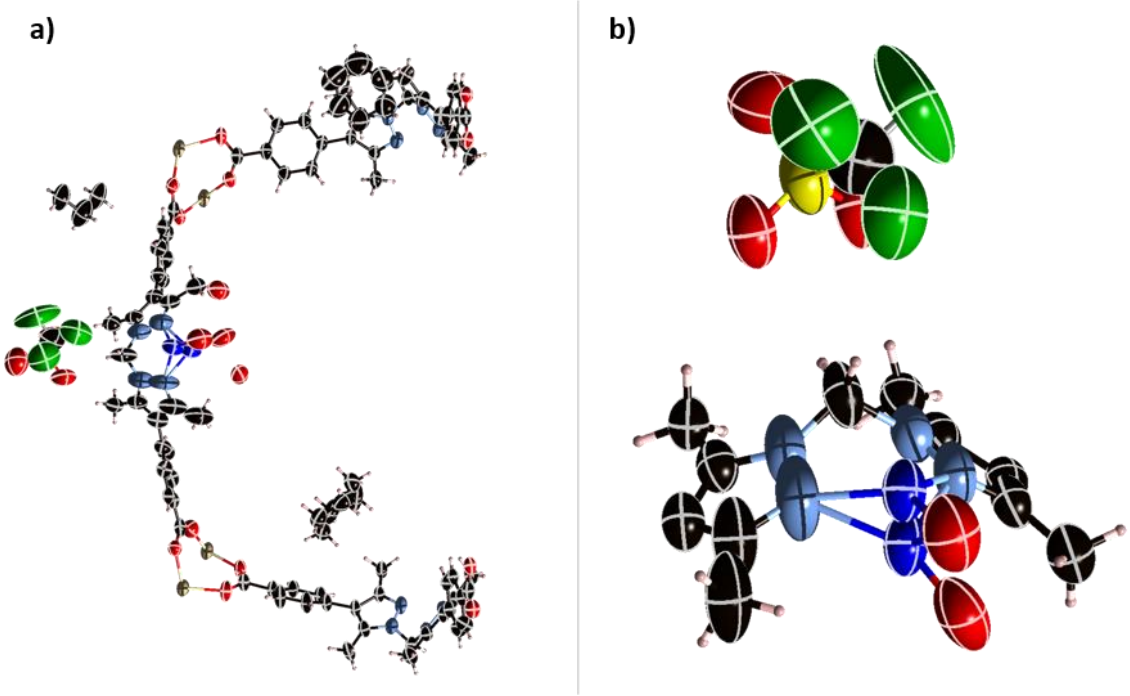

Figure S14: (a) The asymmetric unit of **MnMOF-1**·[Cu(H_2O)]OTf, with all non-hydrogen atoms represented by ellipsoids at the 50% probability level (C, black; H, white; N, light blue; O, red; Cu, dark blue; Mn, beige; S, yellow; F, green). (b) A perspective view of the two Cu(I) chelation site with all non-hydrogen atoms represented by ellipsoids at the 50% probability level.

S3.4 Electron density plots for all structures at the 50% probability level

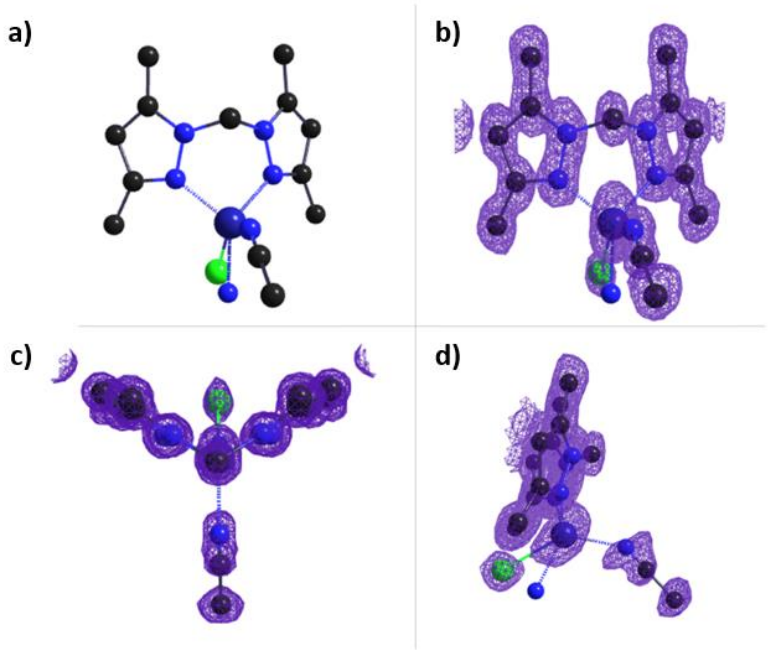

Figure S15: (a) A perspective view of the first chelated Cu(I) complex in **MnMOF-1**·[Cu(CH_3CN)(Cl)], and the overlaid electron density map as viewed from the (b) front, (c) top and (d) side of the complex.

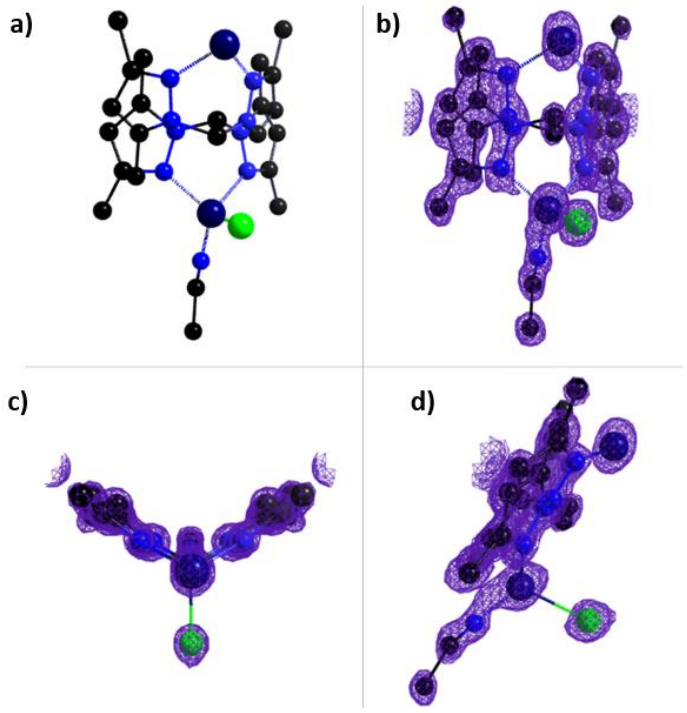

Figure S16: (a) A perspective view of the second chelated Cu(I) complex in **MnMOF-1**·[Cu(CH_3CN)(Cl)], and the overlaid electron density map as viewed from the (b) front, (c) top and (d) side of the complex.

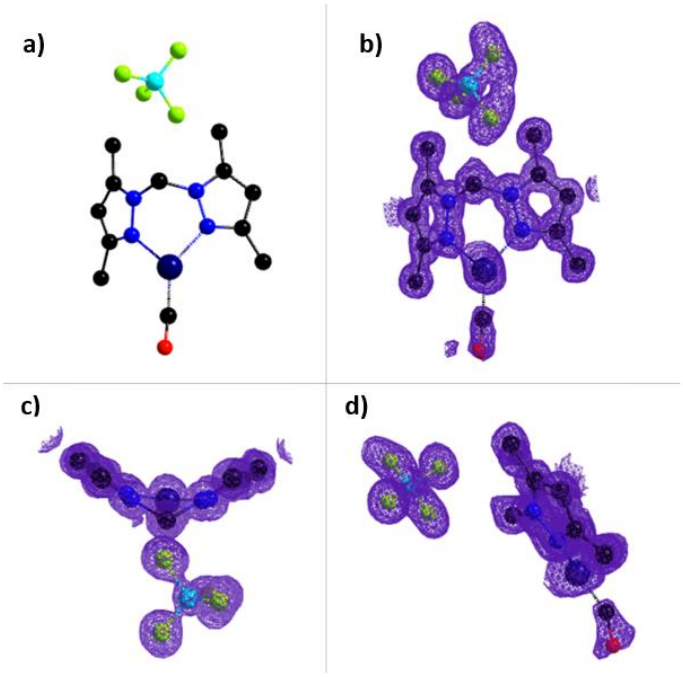

Figure S17: (a) A perspective view of the chelated Cu(I) complex in **MnMOF-1**·[CuCO]BF_4, and the overlaid electron density map as viewed from the (b) front, (c) top and (d) side of the complex.

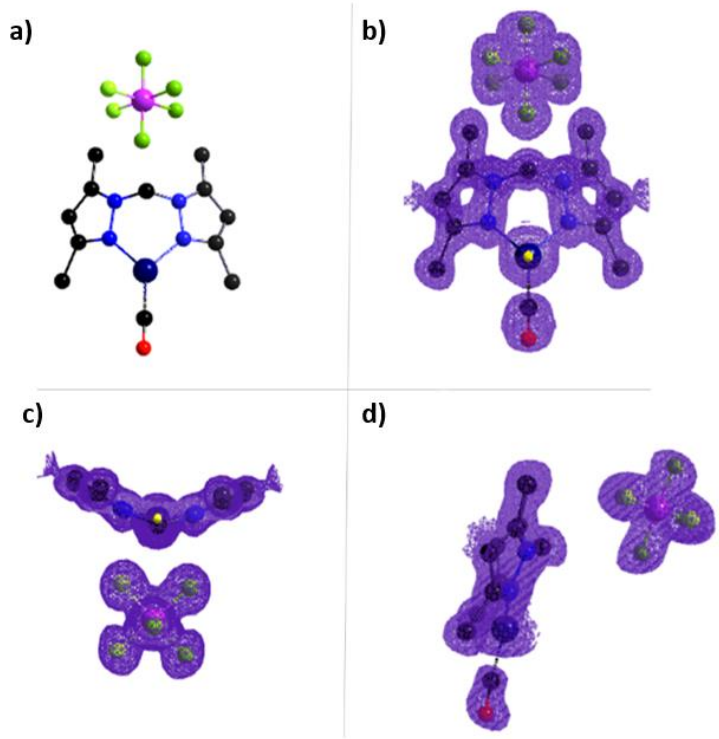

Figure S18: (a) A perspective view of the chelated Cu(I) complex in **MnMOF-1**·[CuCO]PF_6, and the overlaid electron density map as viewed from the (b) front, (c) top and (d) side of the complex.

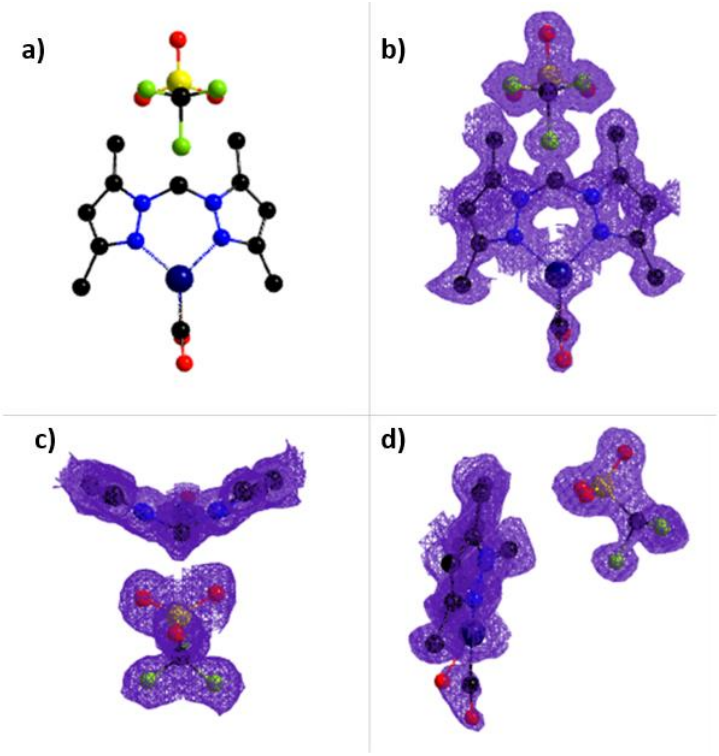

Figure S19: (a) A perspective view of the first chelated Cu(I) complex in **MnMOF-1**·[CuCO]OTf, and the overlaid electron density map as viewed from the (b) front, (c) top and (d) side of the complex.

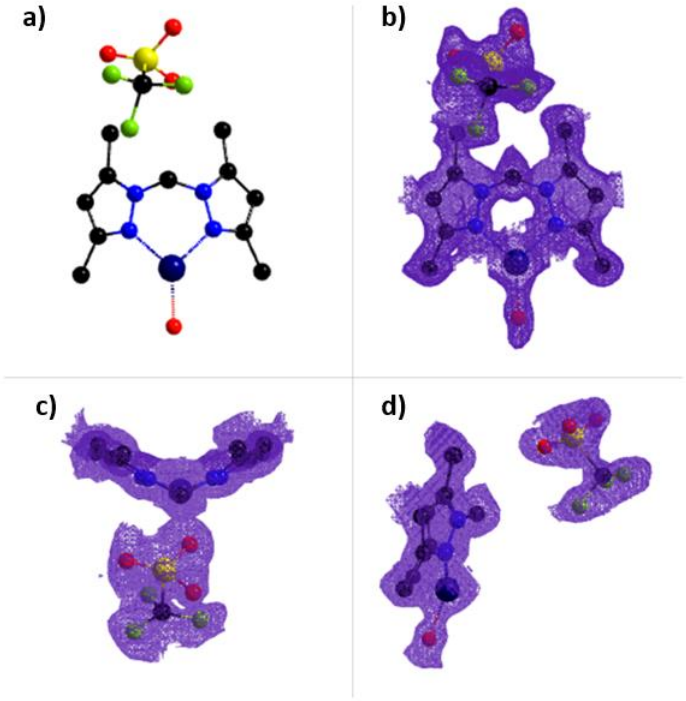

Figure S20: (a) A perspective view of the second chelated Cu(I) complex in **MnMOF-1**·[Cu(H_2O)]OTf, and the overlaid electron density map as viewed from the (b) front, (c) top and (d) side of the complex.

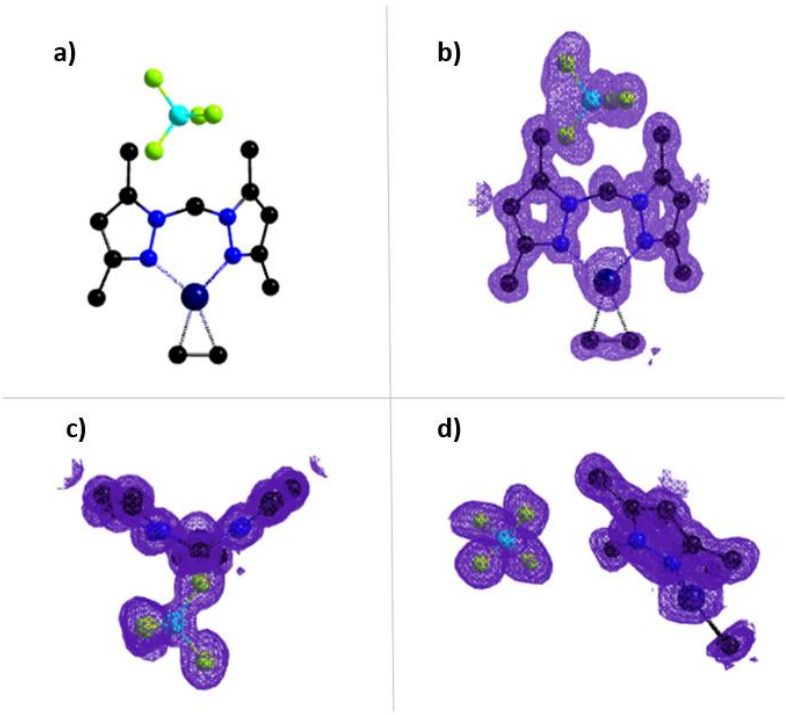

Figure S21: (a) A perspective view of the chelated Cu(I) complex in **MnMOF-1**·[Cu(C_2H_4)]BF_4, and the overlaid electron density map as viewed from the (b) front, (c) top and (d) side of the complex.

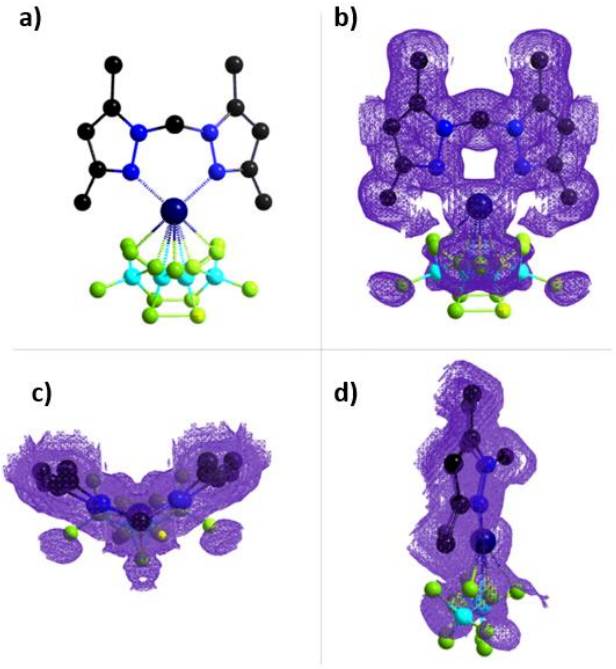

Figure S22: (a) A perspective view of the chelated Cu(I) complex in **MnMOF-1**·[Cu(BF_4)], and the overlaid electron density map as viewed from the (b) front, (c) top and (d) side of the complex. The BF_4 anion is disordered over two crystallographically distinct positions, which gives a total of four positions due to symmetry.

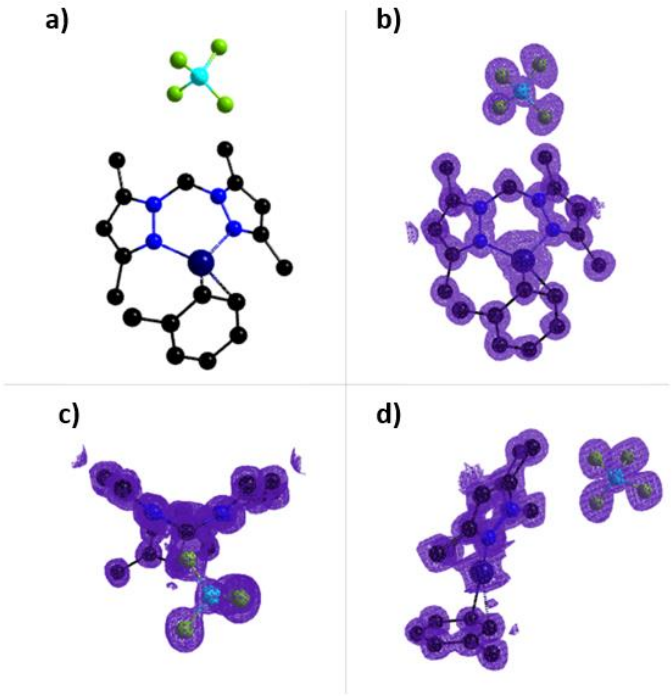

Figure S23: (a) A perspective view of the chelated Cu(I) complex in **MnMOF-1** [Cu(η^2Toluene)]BF_4, and the overlaid electron density map as viewed from the (b) front, (c) top and (d) side of the complex.

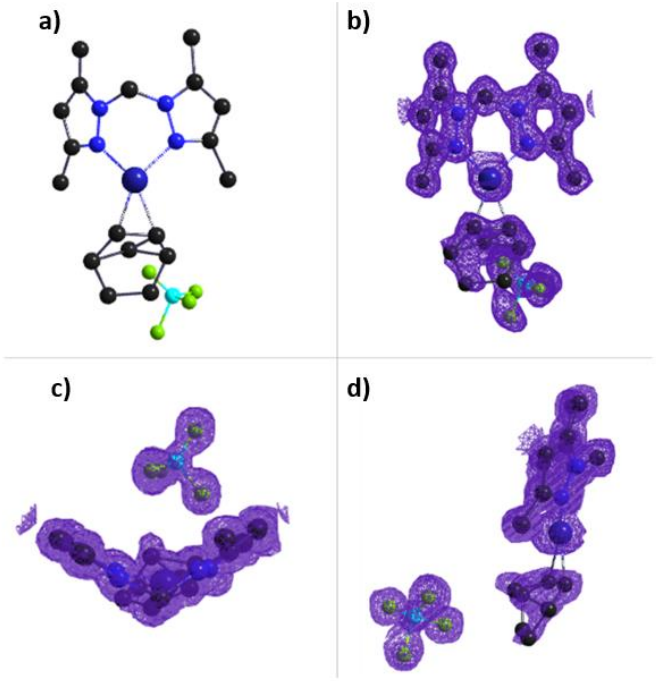

Figure S24: (a) A perspective view of the chelated Cu(I) complex in **MnMOF-1**·[Cu(η^2-NBD)]BF_4, and the overlaid electron density map as viewed from the (b) front, (c) top and (d) side of the complex.

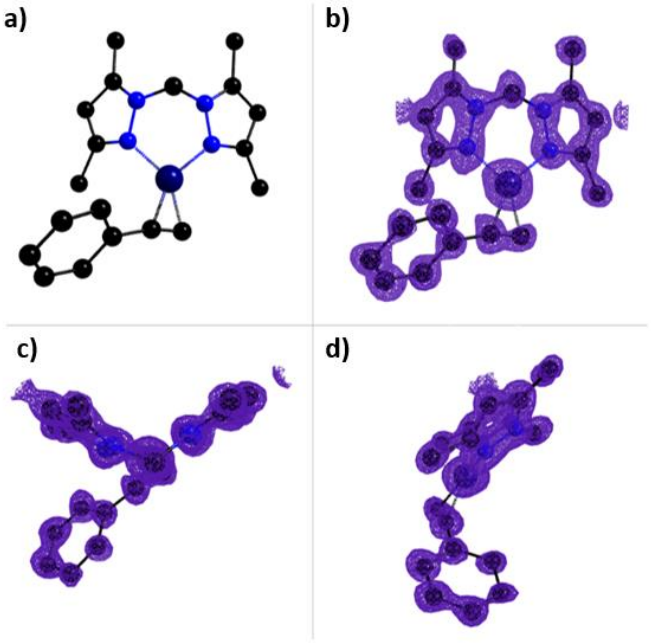

Figure S25: (a) A perspective view of the chelated Cu(I) complex in **MnMOF-1**·[Cu(η^2(HC_2Ph)]BF_4, and the overlaid electron density map as viewed from the (b) front, (c) top and (d) side of the complex.

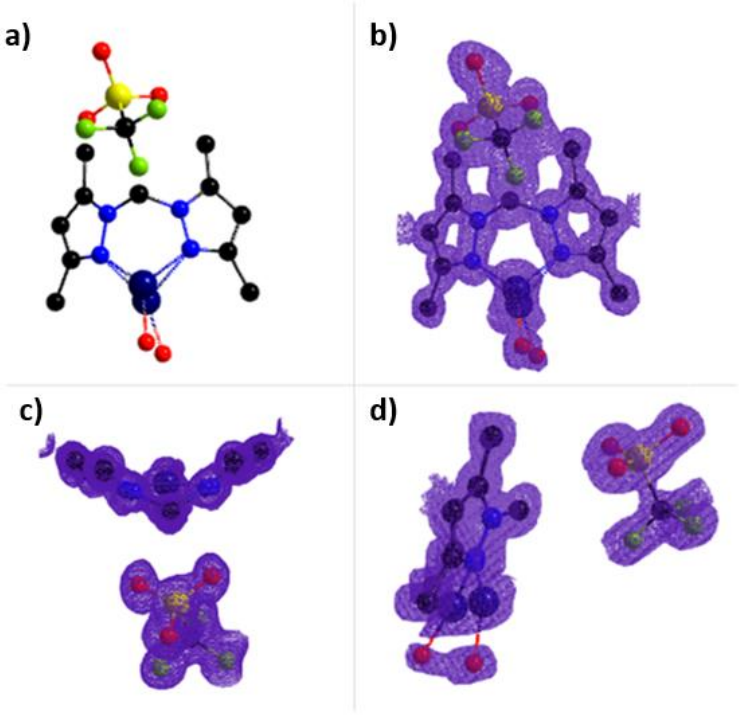

Figure S26: (a) A perspective view of the chelated Cu(I) complex in **MnMOF-1**·[Cu(H_2O)]OTf, and the overlaid electron density map as viewed from the (b) front, (c) top and (d) side of the complex.

S3.5 Tables of X-ray crystallography data collection and refinement parameters

Table S2. Crystallographic data collection and refinement parameters for the metalated forms of **MnMOF-1**.

Sample	**MnMOF-1·[Cu(MeCN)Cl]**	**MnMOF-1·[Cu(CO)]BF_4**	**MnMOF-1·[Cu(CO)]PF_6**	**MnMOF-1·[Cu(CO)]OTf**
Crystallographic Parameter				
Formula	$C_{79}H_{72}ClCuMn_3N_{14}O_{12}$	$C_{76}H_{66}N_{12}O_{13}Mn_3CuF_4B$	$C_{76}H_{66}CuF_6Mn_3N_{12}O_{13}P$	$C_{161.5}H_{150}Cu_2F_6Mn_6N_{24}O_{32}S_2$
FW	1673.31	1670.57	1728.73	3573.89
T, K	100(2)	100(2)	100(2)	100(2)
Wavelength, Å	0.71073	0.71073	0.71073	0.71073
Crystal system, space group	Monoclinic, $P2_1/m$	Monoclinic, $P2_1/c$	Monoclinic, $P2_1/m$	Triclinic, P-1
Z	4	4	4	2
a, Å	12.349(3)	12.379(3)	12.373(3)	12.395(3)
b, Å	32.650(7)	34.724(7)	35.910(7)	25.853(5)
c, Å	25.851(5)	25.893(5)	25.894(5)	35.414(7)
α˚	90	90	90	87.98(3)
β, ˚	94.01(3)	97.79(3)	97.46(3)	88.86(3)
γ˚	90	90	90	81.34(3)
V, Å^3	10397(4)	11027(4)	11408(4)	11211(4)
d_{calc}, g/cm^3	1.069	1.006	1.007	1.059
Absorption coefficient, mm^{-1}	0.636	0.581	0.580	0.594
F(000)	3444.0	3420.0	3532.0	3674.0
Crystal size, mm^3	0.2 × 0.14 × 0.03	0.25 × 0.14 × 0.04	0.19 × 0.12 × 0.02	0.22 × 0.14 × 0.03
2θ range for data collection	2.012 to 53.126	1.974 to 57.998	1.586 to 59.55	1.594 to 64.368
Index range	-15 ≤ h ≤ 15, -41 ≤ k ≤ 41, -31 ≤ l ≤ 31	-16 ≤ h ≤ 16, -42 ≤ k ≤ 42, -34 ≤ l ≤ 34	-16 ≤ h ≤ 16, -42 ≤ k ≤ 43, -34 ≤ l ≤ 35	-14 ≤ h ≤ 14, -34 ≤ k ≤ 34, -47 ≤ l ≤ 47
Reflections collected	155120	136232	138660	172176
Independent reflections	20537 [R_{int} = 0.0922, R_{sigma} = 0.0441]	22483 [R_{int} = 0.0687, R_{sigma} = 0.0335]	22998 [R_{int} = 0.1823, R_{sigma} = 0.1023]	55852 [R_{int} = 0.0897, R_{sigma} = 0.1035]
Data/restraints/parameters	20537/232/1094	22483/74/1003	22998/1587/1042	55852/298/2195
GOF on F^2	1.031	1.085	1.262	1.368
Largest diff. peak and hole, eÅ^{-3}	0.93/-0.93	1.07/-1.93	0.71/-0.82	2.30/-1.10
R_1, [I>2σ(I)]	0.0927	0.1052	0.1657	0.1698
wR_2, all data	0.2693	0.3229	0.4992	0.4640
CCDC Number	2071195	2071198	2071196	2071197

Table S3. Crystallographic data collection and refinement parameters for the metalated forms of **MnMOF-1**.

Sample	**MnMOF-1·[Cu(BF_4)]**	**MnMOF-1·[Cu(NBD)]BF_4**	**MnMOF-1·[Cu(Tol)]BF_4**	**MnMOF-1·[Cu(PhC_2H)]BF_4**
Crystallographic Parameter				
Formula	$C_{75}H_{60}B_{0.8}CuF_{3.2}Mn_3N_{12}O_{12}$	$C_{92.5}H_{83}BCuF_4Mn_3N_{12}O_{12}$	$C_{103}H_{95}BCuF_4Mn_3N_{12}O_{12}$	$C_{91}H_{78}CuMn_3N_{12}O_{12}$
FW	1619.15	1869.87	2008.07	1760.01
T, K	100(2)	100.0	100	100.15
Wavelength, Å	0.71073	0.71073	0.71073	0.71073
Crystal system, space group	Monoclinic, $P2_1/m$	Monoclinic, $P2_1/c$	Monoclinic, $P2_1/c$	Triclinic, P-1
Z	2	4	4	2
a, Å	12.437(3)	12.356(3)	12.367(3)	12.325(3)
b, Å	34.935(7)	34.639(7)	34.582(7)	12.935(3)
c, Å	12.903(3)	25.985(5)	25.915(5)	34.437(7)
α˚	90	90	90	90.50(3)
β, ˚	98.27(3)	96.94(3)	97.89(3)	92.33(3)
γ˚	90	90	90	99.98(3)
V, Å^3	5548(2)	11040(4)	10978(4)	5402(2)
d_{calc}, g/cm^3	0.969	1.125	1.215	1.082
Absorption coefficient, mm^{-1}	0.574	0.587	0.595	0.591
F(000)	1654.0	3852.0	4152.0	1816.0
Crystal size, mm^3	0.18 × 0.11 × 0.02	0.19 × 0.09 × 0.04	0.19 × 0.08 × 0.03	0.17 x 0.07 x 0.03
2θ range for data collection	2.332 to 63.762	1.968 to 64.284	1.976 to 64.316	2.368 to 63.708
Index range	-16 ≤ h ≤ 16, -47 ≤ k ≤ 47, -15 ≤ l ≤ 15	-17 ≤ h ≤ 17, -46 ≤ k ≤ 46, -35 ≤ l ≤ 34	-14 ≤ h ≤ 14, -46 ≤ k ≤ 46, -35 ≤ l ≤ 35	-18 ≤ h ≤ 18, -17 ≤ k ≤ 17, -46 ≤ l ≤ 46
Reflections collected	85376	189007	198103	83918
Independent reflections	14627 [R_{int} = 0.0994, R_{sigma} = 0.0699]	29194 [R_{int} = 0.0955, R_{sigma} = 0.0573]	29451 [R_{int} = 0.0728, R_{sigma} = 0.0377]	24783 [R_{int} = 0.1420, R_{sigma} = 0.1237]
Data/restraints/parameters	14627/141/539	29194/251/1157	29451/68/1240	24783/604/1019
GOF on F^2	1.351	1.040	1.053	1.388
Largest diff. peak and hole, eÅ^{-3}	0.83/-1.22	1.05/-1.17	0.88/-0.77	0.56/-1.25
R_1, [I>2σ(I)]	0.1432	0.0892	0.0602	0.2025
wR_2, all data	0.4647	0.2966	0.1849	0.5691
CCDC Number	2071201	2071194	2071203	2071200

Table S4. Crystallographic data collection and refinement parameters for the metalated forms of **MnMOF-1**.

Sample	**MnMOF-1·[Cu(H_2O)]OTf**	**MnMOF-1·[Cu(C_2H_4)]BF_4**
Crystallographic Parameter		
Formula	$C_{91}H_{96}Cu_{1.02}F_3Mn_3N_{12}O_{17.5}S$	$C_{77}H_{70}BCuF_4Mn_3N_{12}O_{12}$
FW	1956.48	1670.62
T, K	100(2)	100(2)
Wavelength, Å	0.71073	0.71073
Crystal system, space group	Triclinic, P-1	Monoclinic, $P2_1/c$
Z	2	4
a, Å	12.456(3)	12.298(3)
b, Å	12.898(3)	34.353(7)
c, Å	35.140(7)	25.793(5)
α˚	88.09(3)	90
β, ˚	85.82(3)	98.30(3)
γ˚	79.80(3)	90
V, Å^3	5540(2)	10783(4)
d_{calc}, g/cm^3	1.173	1.029
Absorption coefficient, mm^{-1}	0.612	0.594
F(000)	2027.0	3428.0
Crystal size, mm^3	0.23 × 0.14 × 0.03	0.2 × 0.07 × 0.02
2θ range for data collection	2.324 to 64.332	1.988 to 58.356
Index range	-16 ≤ h ≤ 16, -19 ≤ k ≤ 19, -47 ≤ l ≤ 47	-16 ≤ h ≤ 16, -45 ≤ k ≤ 45, -34 ≤ l ≤ 34
Reflections collected	96363	139847
Independent reflections	28163 [R_{int} = 0.0551, R_{sigma} = 0.0554]	23497 [R_{int} = 0.0750, R_{sigma} = 0.0444]
Data/restraints/parameters	28163/253/1191	23497/50/999
GOF on F^2	1.295	1.297
Largest diff. peak and hole, eÅ^{-3}	1.12/-1.21	1.59/-0.75
R_1, [I>2σ(I)]	0.1100	0.1074
wR_2, all data	0.3711	0.3510
CCDC Number	2071202	2071199

S4.0 Isotherm data

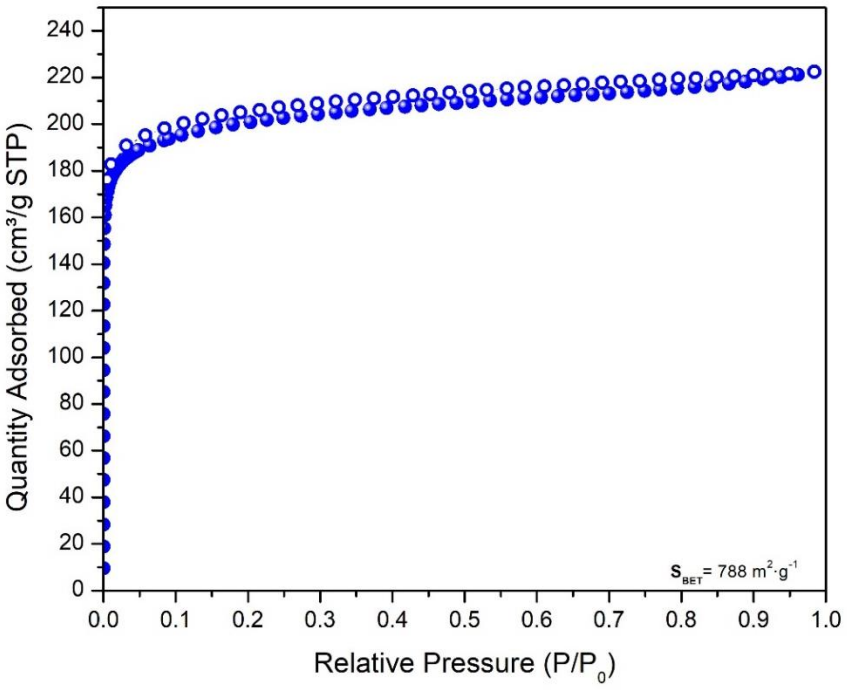

Figure S27: N_2 isotherm data collected on **MnMOF-1**·[CuCO]BF_4 at 77K, after activation from dry pentane at RT for 2 hours. Coloured circles represent adsorption, open circles represent desorption.

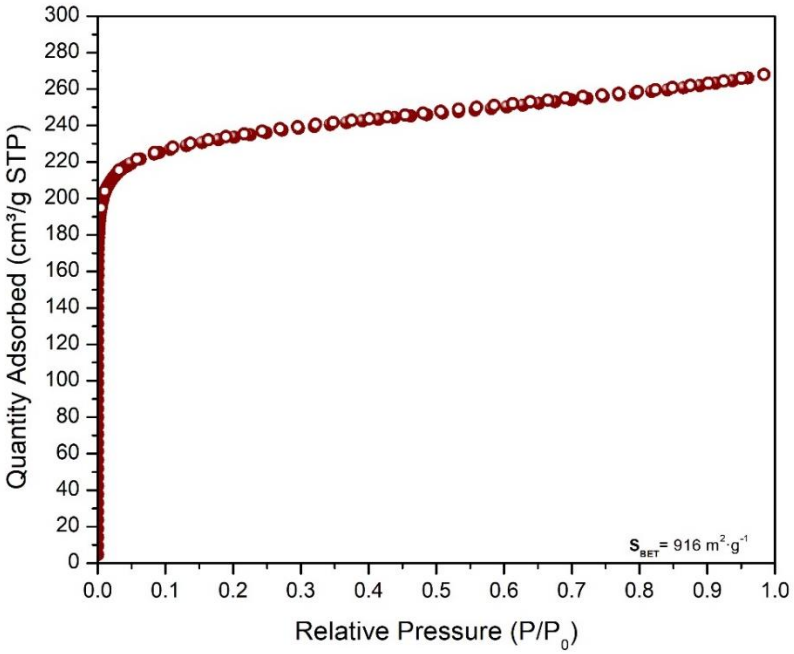

Figure S28: N_2 isotherm data collected on **MnMOF-1**·[CuCO]PF_6 at 77K, after activation from dry pentane at RT for 2 hours. Coloured circles represent adsorption, open circles represent desorption.

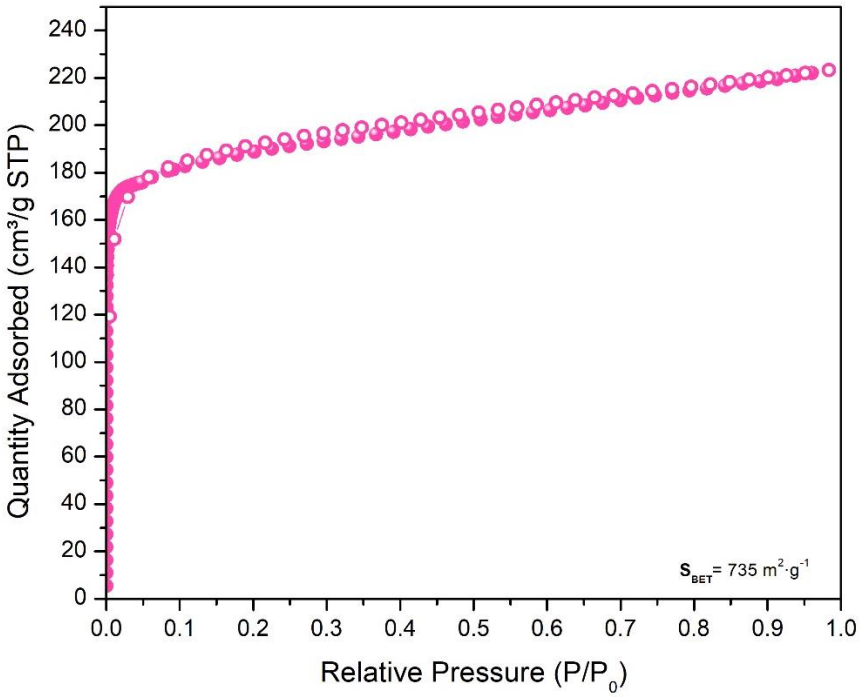

Figure S29: N_2 isotherm data collected on **MnMOF-1**·[CuCO]OTf at 77K, after activation from dry pentane at RT for 2 hours. Coloured circles represent adsorption, open circles represent desorption.

S5.0 Infrared (IR) spectroscopy

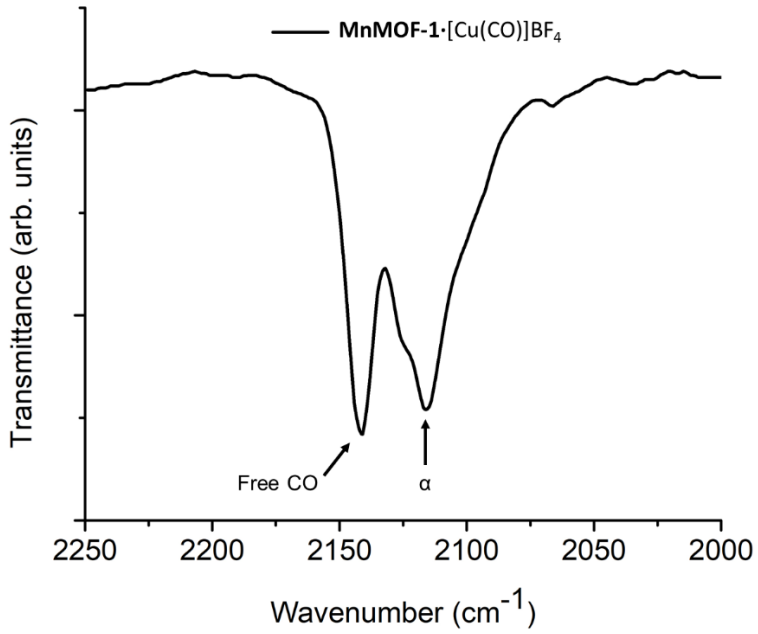

Figure S30: Infra-red spectrum (neat) of **MnMOF-1**·[CuCO]BF_4 following exposure to vacuum for two hours (CO loss) and dosing with carbon monoxide to regenerate the **MnMOF-1**·[Cu(CO)]BF_4. To remove as much excess CO as possible, the sample chamber was briefly flushed with Argon. The IR spectrum displays the copper carbonyl stretch observed at 2105 cm^{-1} and excess free CO trapped in the MOF pellet.

S6.0 Formation of MnMOF-1·[Cu(OH_2)]OTf

We noted that when insufficiently dried triflate was used to perform the anion metathesis ligand exchange of **MnMOF-1**·[Cu(MeCN)Cl] in presence of CO, a trigonal planar Cu(I) aqua complex was formed. We postulate that water entered via the highly hydroscopic NaOTf salt during handling. As outlined in S3.2 and in Figure S8, **MnMOF-1**·[Cu(CO)]OTf features a mixture of trigonal planar Cu(CO) sites and trigonal planar Cu(OH_2) sites, indicating that complete prevention of water coordination (presumably from the hydroscopic NaOTf salt) is difficult. In one instance, presumably due to excessive moisture present in the NaOTf salt, a sample of **MnMOF-1**·[Cu(OH_2)]OTf was obtained in which negligible coordinated CO is present. The crystal structure revealed a trigonal planar Cu(OH_2) moiety, commensurate with the minor component observed in **MnMOF-1**·[Cu(CO)]OTf, with Cu-OH_2 bond length of 1.890(16). The triflate anion is located in the MOF pore as observed in **MnMOF-1**·[Cu(CO)]OTf.

S7.0 In-situ IR spectroscopy cell

The *In-situ* FTIR cell (Figure S31 used to assess the stability of **1**·[CuCO]BF_4 was developed in-house.

In-situ FTIR cell assembly:

65mm x 16mm, 304ss, 2 Port, OR, and Tapped, with an internal volume of 25 mL. Mini Ball Valve, BRS, N/P SCD M/ F ¼" 8MM connected to both ports. Stainless Steel Swagelok Tube Fitting, Male Elbow, 1/4 in. Tube OD x 1/4 in. Male ISO Tapered Thread connected to Mini Ball Valves.

Viewport Flange - 65mm x 16mm, 304ss, OR, and bolted to IR Sampling Chamber backside using M3 x 16 304ss Hex. Socket Cap Screws.

Lens – NaCl disks 25.4mm x 5.1mm and fitted to inside of Viewport Flange bore.

Lens Cap - 40mm x 16mm, 304ss, OR, and bolted to Viewport Flange outer face using M3 x 10 304ss Hex. Socket Cap Screws.

Lens: 25.4mm x 5.1mm Quartz and fitted to inside IR Sampling Chamber frontside bore.

Slide Holder - 50.4mm x 76.5mm x 5.5mm x 16mm BORE, 304ss, OR, and bolted to IR Sampling Chamber frontside using M3 x 10 304ss Countersink Head Hex. Screws.

Sample Holder Assembly:

Front Flange - 37mm x 16mm, Tapped, 304ss and bolted internally to IR Sampling Chamber using M2 x 8 304ss Hex. Socket Cap Screws. Back Flange – 37mm x 16mm, Clearance, 304ss 2 x 25.4mm x 5.1mm thick lenses clamped together, face to face, using M3 x 8 304ss Hex. Socket Cap Screws.

Notes: All parts thoroughly cleaned before assembly.

MS-PTS-50 Swagelok SWAK Anerobic Thread Sealant 50cm^3 Tube was applied to all male threads before assembly and allowed to cure for 24 hours.

IR Sampling Cell Assembly pressure tested to 80psi (5.5bar) with compressed air and Helium Leak Tested.

To load the sample, a NaCl disk is placed into the chamber. One outlet is connected to a glass manifold pressurised with Argon (Hg pressure), an inverted funnel is placed over the chamber to maintain an Argon atmosphere while allowing access to the chamber for loading the sample. A narrow paper 'funnel' is positioned in the small opening of the inverted funnel, such that it rests on the middle of the NaCl disk. The dry sample is carefully dropped through the paper funnel onto in the middle of the NaCl disk (neat) while maintaining the Argon blanket within the chamber. A second NaCl disk is placed on top of the sample. Maintaining constant Ar flow the chamber is sealed and an initial spectrum is collected before the chamber is placed under vacuum.

Figure S31: *In-situ* FTIR cell with double tap assembly.

S8.0 References

1. McPhillips, T.; McPhillips, S.; Chiu, H.; Cohen, A. E.; Deacon, A. M.; Ellis, P. J.; Garman, E.; Gonzalez, A.; Sauter, N. K.; Phizackerley, R. P.; Soltis, S. M.; Kuhn, P., Blue-Ice and the Distributed Control System software for data acquisition and instrument control at macromolecular crystallography beamlines. *J. Synchrotron Radiat.* **2002,** *9*, 401-406.
2. Cowieson, N. P.; Aragao, D.; Clift, M.; Ericsson, D. J.; Gee, C.; Harrop, S. J.; Mudie, N.; Panjikar, S.; Price, J. R.; Riboldi-Tunnicliffe, A.; Williamson, R.; Caradoc-Davies, T., MX1: a bending-magnet crystallography beamline serving both chemical and macromolecular crystallography communities at the Australian Synchrotron. *J. Synchrotron Radiat.* **2015,** *22* (1), 187-190.
3. Aragao, D.; Aishima, J.; Cherukuvada, H.; Clarken, R.; Clift, M.; Cowieson, N. P.; Ericsson, D. J.; Gee, C. L.; Macedo, S.; Mudie, N.; Panjikar, S.; Price, J. R.; Riboldi-Tunnicliffe, A.; Rostan, R.; Williamson, R.; Caradoc-Davies, T. T., MX2: a high-flux undulator microfocus beamline serving both the chemical and macromolecular crystallography communities at the Australian Synchrotron. *J. Synchrotron Rad.* **2018,** *25* (3), 885-891.
4. Sheldrick, G., A short history of SHELX. *Acta. Crystallogr. A* **2008,** *64* (1), 112-122.
5. Sheldrick, G., SHELXT - Integrated space-group and crystal-structure determination. *Acta. Crystallogr. A* **2015,** *71* (1), 3-8.
6. Sheldrick, G. M., Crystal structure refinement with SHELXL. *Acta. Crystallogr. C* **2015,** *71* (Pt 1), 3-8.
7. Barbour, L. J., X-Seed — A Software Tool for Supramolecular Crystallography. *J. Supramol. Chem.* **2001,** *1* (4), 189-191.
8. Dolomanov, O. V.; Bourhis, L. J.; Gildea, R. J.; Howard, J. A. K.; Puschmann, H., OLEX2: a complete structure solution, refinement and analysis program. *J. Appl. Crystallogr.* **2009,** *42* (2), 339-341.
9. Spek, A. L., PLATON SQUEEZE: a tool for the calculation of the disordered solvent contribution to the calculated structure factors. *Acta. Crystallogr. C* **2015,** *71* (Pt 1), 9-18.